Mrx6 regulates mitochondrial DNA copy number in *Saccharomyces cerevisiae* by engaging the evolutionarily conserved Lon protease Pim1

Aylin Göke[a], Simon Schrott[b], Arda Mizrak[c], Vladislav Belyy[a], Christof Osman[a,b,†,*], and Peter Walter[a,*]

[a]Howard Hughes Medical Institute and Department of Biochemistry and Biophysics and [c]Department of Physiology, University of California, San Francisco, San Francisco, CA 94143; [b]Faculty of Biology, Ludwig-Maximilian-Universität München, 82152 Planegg-Martinsried, Germany

ABSTRACT **Mitochondrial function depends crucially on the maintenance of multiple mitochondrial DNA (mtDNA) copies. Surprisingly, the cellular mechanisms regulating mtDNA copy number remain poorly understood. Through a systematic high-throughput approach in *Saccharomyces cerevisiae*, we determined mtDNA–to–nuclear DNA ratios in 5148 strains lacking nonessential genes. The screen revealed *MRX6*, a largely uncharacterized gene, whose deletion resulted in a marked increase in mtDNA levels, while maintaining wild type–like mitochondrial structure and cell size. Quantitative superresolution imaging revealed that deletion of *MRX6* alters both the size and the spatial distribution of mtDNA nucleoids. We demonstrate that Mrx6 partially colocalizes with mtDNA within mitochondria and interacts with the conserved Lon protease Pim1 in a complex that also includes Mam33 and the Mrx6-related protein Pet20. Acute depletion of Pim1 phenocopied the high mtDNA levels observed in Δ*mrx6* cells. No further increase in mtDNA copy number was observed upon depletion of Pim1 in Δ*mrx6* cells, revealing an epistatic relationship between Pim1 and Mrx6. Human and bacterial Lon proteases regulate DNA replication by degrading replication initiation factors, suggesting a model in which Pim1 acts similarly with the Mrx6 complex, providing a scaffold linking it to mtDNA.**

Monitoring Editor
Thomas D. Fox
Cornell University

Received: Aug 26, 2019
Accepted: Sep 10, 2019

This article was published online ahead of print in MBoC in Press (http://www.molbiolcell.org/cgi/doi/10.1091/mbc.E19-08-0470) on September 18, 2019.

The authors declare no competing financial interests.

Author contributions: A.G., S.S., A.M., V.B., C.O., and P.W. conceived the project; P.W. acquired funding; C.O. and P.W. provided resources; A.G. and C.O. curated the data; A.G., S.S., V.B., A.M., and C.O. performed formal analysis; A.G., S.S., and C.O. provided validation, investigation, and visualization; A.G., S.S., and C.O. were responsible for methodology; A.M., V.B., and C.O. managed software; V.B., C.O., and P.W. supervised; A.G. and C.O. wrote the original draft; and A.G., S.S., V.B., C.O., and P.W. reviewed and edited the manuscript.

†Present address: Faculty of Biology, Ludwig-Maximilian-Universität München, 82152 Planegg-Martinsried, Germany.

*Address correspondence to: Peter Walter (peter@walterlab.ucsf.edu); Christof Osman (osman@biologie.uni-muenchen.de).

Abbreviations used: BFP, blue fluorescent protein; DAPI, 4′,6-diamidino-2-phenylindole; DMSO, dimethyl sulfoxide; FCCP, carbonyl cyanide-4-(trifluoromethoxy) phenylhydrazone; MCC, Manders colocalization coefficient; mtDNA, mitochondrial DNA; nDNA, nuclear DNA; PCC, Pearson's correlation coefficient; qPCR, quantitative PCR; SD, synthetic dextrose; SI, structured illumination; SSC-H, side scatter height; YPD, yeast extract peptone dextrose; YPG, yeast extract peptone ethanol glycerol; WT, wild type.

INTRODUCTION

Mitochondria are endosymbiotic organelles that carry multiple copies of their own genomes, encoding proteins required for oxidative phosphorylation and respiratory metabolism. Mitochondrial DNA (mtDNA) copies are packaged together with several mtDNA-binding proteins to form nucleoids that distribute throughout the mitochondrial network and display a semiregular spacing in the mitochondrial network (Chen and Butow, 2005; Brown *et al.*, 2011; Osman *et al.*, 2015; Jajoo *et al.*, 2016; Lewis *et al.*, 2016). The copy number of mtDNA in each cell is maintained within a narrow range (Chen and Butow, 2005; Clay Montier *et al.*, 2009). Previous studies reported that *Saccharomyces cerevisiae* cells maintain ~40–60 nucleoids, each carrying ~1–2 mtDNA copies (Chen and Butow, 2005), although some reviews cite up to 10 copies per nucleoid (Lipinski *et al.*, 2010). Mammalian cells can contain thousands of nucleoids, depending on tissue type (Williams, 1986; Miller *et al.*, 2003). Recent superresolution-microscopy experiments demonstrated that most nucleoids contain only a single mtDNA copy (Kukat *et al.*, 2011).

Altered levels of mtDNA are linked to a variety of diseases, including neurodegenerative and metabolic diseases and various

types of cancer (Liu *et al.*, 2006; Clay Montier *et al.*, 2009; Ylikallio *et al.*, 2010; Yu, 2011; Kornblum *et al.*, 2013; Mengel-From *et al.*, 2014; Pyle *et al.*, 2016). Furthermore, increasing mtDNA copy number has been suggested to help cells ameliorate the effect of myocardial infarction in mice (Ikeda *et al.*, 2015). Despite their physiological importance, the cellular mechanisms that regulate mtDNA copy number remain poorly understood. Previous genetic screens designed to identify new components that control mtDNA copy number focused on mutants that lead to mtDNA loss and identified numerous components important for mtDNA maintenance (Fukuoh *et al.*, 2014; Zhang and Singh, 2014). However, loss of mtDNA is often caused by secondary effects due to compromised mitochondrial function (Lipinski *et al.*, 2010). Therefore, the question of how mtDNA copy number is regulated to remain within a narrow window has remained largely unanswered.

To elucidate how mtDNA levels are sustained at their physiological set point, we determined mtDNA levels in a yeast deletion library. This screen revealed the gene *MRX6* as a crucial component of mtDNA copy number control.

RESULTS

A genetic screen identifies cellular machineries regulating mtDNA copy number

We systematically determined the amount of mtDNA relative to nuclear DNA (nDNA) in 5148 strains of a yeast gene-deletion library generated in S288c cells, each lacking a different nonessential gene (*Saccharomyces* Genome Deletion Project; Giaever *et al.*, 2002). Mutant colonies grown on rich medium were transferred to nylon membranes, lysed, and hybridized with two different sets of fluorescent probes specific for mtDNA and nDNA, respectively (Figure 1, A and B). We determined the fluorescence intensity of both probes and calculated the mtDNA/nDNA ratio for each mutant. Mutants were classified into three categories: 1) mutants that contained an increased mtDNA/nDNA ratio, 2) mutants that maintained their mtDNA/nDNA ratio similarly to wild-type cells (WT), and 3) mutants that lost the majority or all of mtDNA (Figure 1C; Supplemental Figure1A; Supplemental Table 1). The following observations indicate that this screen faithfully reports on mtDNA levels: ~80% of mutants falling into the third category were previously described to be respiratory-deficient or defective in maintenance of mtDNA (Supplemental Figure 1B; Supplemental Table 1B). Furthermore, mutants lacking the genes *SML1*, *RRM3*, and *RFX1*, which were previously reported to contain elevated levels of mtDNA (Taylor *et al.*, 2005), were also identified in our analysis as having increased mtDNA/nDNA ratios (Supplemental Table 1A).

Loss or reduction of mtDNA can result in various mitochondrial defects (Lipinski *et al.*, 2010). Therefore, we focused on mutants that displayed higher mtDNA/nDNA ratios, which are more likely to be indicative of a defect in mDNA–copy number regulation. To validate our hits, we repeated the colony blot hybridization with the initially identified candidates (167 mutants) and selected 91 mutants for which increased mtDNA levels were reproduced for further analysis (Supplemental Figure 1C; Supplemental Table 1C). As yeast colonies on agar plates consist of heterogeneous cell populations that differ in metabolic and respiratory states (Traven *et al.*, 2012), we isolated genomic DNA from the 91 mutants grown in liquid cultures from early to midlogarithmic phase and quantified their mtDNA levels relative to those of WT cells by quantitative PCR (qPCR). A majority of the mutants (73 of 91) showed a >50% increase in the mtDNA/nDNA ratio (Supplemental Table 1D).

In yeast, mtDNA copy number correlates linearly with the length of the mitochondrial network (Osman *et al.*, 2015). Furthermore, mitochondrial network volume correlates linearly with cell volume (Rafelski *et al.*, 2012). For this reason, elevated mtDNA levels could result as a secondary effect of increased cell size, as would be expected, for example, in mutants that affect cell cycle progression (Conrad and Newlon, 1982). To eliminate such mutants from our analyses, we determined the cell size of the 91 candidates by flow cytometry using side-scattered light as a proxy. Indeed, a majority of the mutants showed an increase in cell size (Figure 1D; Supplemental Table 1D). By contrast, nine mutants displayed cell sizes that were within 10% of the value obtained for WT cells, making them likely candidates to be involved in mtDNA–copy number regulation (Figure 1E).

Deletion of *MRX6*, a largely uncharacterized gene, increases mtDNA copy number

From the genes whose deletion resulted in increased mtDNA levels without altering cell size, we chose to focus on *MRX6* because 1) the mtDNA/nDNA ratio increase in Δ*mrx6* cells was the largest among the mutants that do not affect cell size (Figure 1D), 2) Mrx6 has a predicted mitochondrial-targeting sequence, and 3) Mrx6 belongs to an uncharacterized protein family. To verify that increased levels of mtDNA were linked to deletion of *MRX6* and not caused by second-site mutations in the library strain, we engineered a fresh Δ*mrx6* deletion strain, which reproduced the phenotype of strongly elevated mtDNA levels (Figure 2A). While we observed an ~2.5-fold increase in the library strain, we observed only an ~1.5-fold increase in the newly generated strain. We attribute this difference to the fact that the strains were generated in different yeast backgrounds (S288c vs. W303) carrying different amounts of mtDNA (Connelly and Akey, 2012) and/or to a possibility of aggravating second-site mutations in the deletion library strain. The 1.5-fold increase in Δ*mrx6* cells versus WT cells was statistically significant ($p < 0.01$). For the remaining experiments, we used the freshly generated Δ*mrx6* W303 strain.

Previous studies reported that mtDNA abundance ranges from 25 to 100 copies per cell depending on the strain and growth conditions (MacAlpine *et al.*, 2000; Chen and Butow, 2005). To obtain an accurate quantification of mtDNA levels in our strains, we determined the absolute mtDNA copy number by qPCR analysis using oligonucleotides specific for nuclearly encoded *ACT1* and mitochondrially encoded *COX1*. To this end, we cloned ~1 kb fragments of *ACT1* and *COX1* into plasmids, which we used as standards to correlate threshold PCR cycle values with copy number. According to these measurements, we conclude that haploid WT cells have 21 (±4) copies of mtDNA, whereas Δ*mrx6* cells carry 32 (±5) copies (Figure 2A).

We next tested whether deletion of *MRX6* compromises mitochondrial function. To this end, we monitored growth of Δ*mrx6* cells on a nonfermentable carbon source, which necessitates a functional respiratory chain. Δ*mrx6* cells did not exhibit any growth phenotype, in contrast to WT cells (Figure 2B). Next, we tested mtDNA levels in WT and Δ*mrx6* cells grown under different conditions, such as 1) on a nonfermentable carbon source, 2) under oxidizing stress, and 3) in the presence of an electron-transport chain uncoupler (Figure 2, C and D). These analyses revealed that the absence of *MRX6* leads to a robust increase of mtDNA under all conditions tested and that it occurs independent of metabolic or stress adaptation responses.

As deletion of *MRX6 increased* mtDNA levels, we next asked whether overexpression of Mrx6 would *decrease* them. We overexpressed a C-terminally myc-tagged version of Mrx6 (Mrx6-myc; Supplemental Figure 2) but did not observe altered mtDNA levels

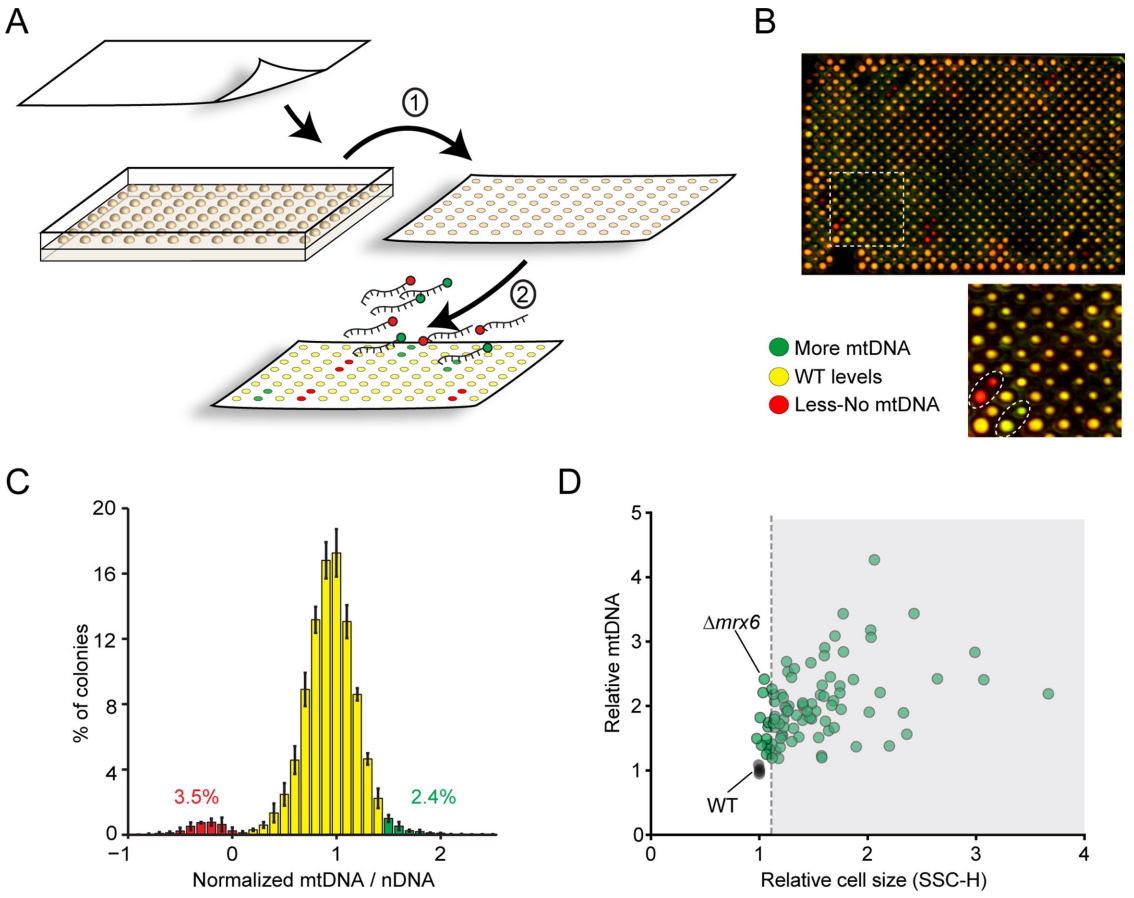

E

Gene ID	Gene name	Relative mtDNA (qPCR)	SEM (qPCR)	Relative cell size (SSC-H)	SEM (SSC-H)
YNL295W	*MRX6*	2.42	0.13	1.05	0.00
YOL076W	*MDM20*	2.26	0.22	1.12	0.07
YOR114W	*YOR114W*	2.21	0.39	1.03	0.01
YDR448W	*ADA2*	1.82	0.07	1.01	0.04
YLR176C	*RFX1*	1.74	0.06	1.09	0.01
YDL049C	*KNH1*	1.68	0.09	1.08	0.01
YGR252W	*GCN5*	1.50	0.08	0.98	0.07
YMR100W	*MUB1*	1.49	0.27	1.07	0.00
YBR194W	*AIM4*	1.39	0.09	1.02	0.01

FIGURE 1: Forward genetic screen to identify cellular machinery regulating mtDNA copy number. (A) Schematic illustration of the genetic screen. Mutants of the yeast deletion library were grown on agar plates (fermentable rich media, YPD) and transferred to nylon membranes (1), lysed, and hybridized with two sets of fluorescent probes specific for mitochondrial DNA (green) or nuclear DNA (red) (2). (B) Scan of a colony blot is shown as an overlay of two channels. Each mutant has its replicate on the diagonal. Mutants with mtDNA/nDNA ratios similar to WT appear yellow, whereas mutants with increased or decreased mtDNA levels are depicted in green and red, respectively. (C) Histogram showing distribution of relative fold changes in mtDNA/nDNA ratios of the mutants. Error bars indicate standard deviations (SD) of three independent colony blot experiments ($n = 3$). Out of total mutants, 2.4% showed an increase in mtDNA copy number by at least 50% (green) and 3.5% lost the majority of or entirely lack mtDNA (red). mtDNA/nDNA ratios below zero are due to subtraction of colony auto-fluorescence from hybridization signal (Supplemental Figure 1; for the list of mutants see Supplemental Table 1). (D) mtDNA levels of 91 hits identified by colony blot screens were verified by qPCR, shown as an average of two independent experiments. Cell sizes of mutants were determined by flow cytometry using SSC-H. Values are relative to WT (see Supplemental Table 1D). Three mutants showing budding defects were omitted from analysis; WT shown in black. Dashed line marks 10% cutoff. Cells were grown in YPD. (E) List of genes identified in this study; their deletion mutants led to an increase in mtDNA copy number but their cell size remained within 10% of WT. mtDNA levels and cell sizes were determined relative to WT ($n = 2$).

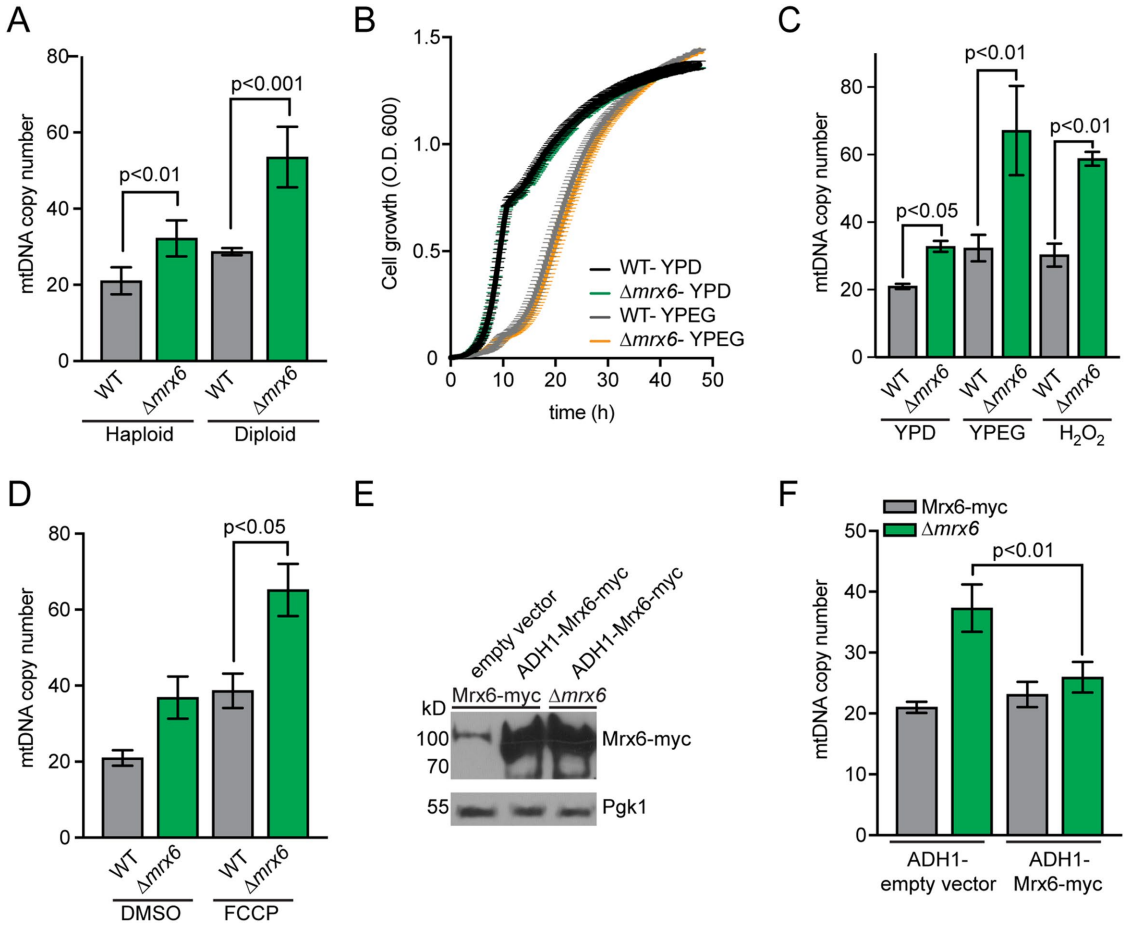

FIGURE 2: Deletion of an uncharacterized gene, *MRX6*, increases mtDNA copy number. (A) qPCR analyses of mtDNA copy number in haploid and diploid W303 cells lacking *MRX6*. Cells were grown in YPD. Error bars indicate SD ($n = 4$). (B) Growth curves of WT and Δ*mrx6* cells grown in YPD or YPEG (rich media with ethanol and glycerol; $n = 2$). (C) qPCR analyses of mtDNA levels in WT and Δ*mrx6* cells grown in YPD or YPEG or treated with 0.5 mM H_2O_2 in YPD for 1 h. (YPD and YPD+ H_2O_2, $n = 2$; YPEG, $n = 4$.) (D) qPCR analyses of mtDNA levels in WT and Δ*mrx6* cells grown in YPD and treated with DMSO or FCCP (5μg/ml) for 1 h ($n = 2$). (E) Western blot analyses of Mrx6-myc levels in cells that either express Mrx6-myc or lack Mrx6, transformed with an empty vector or a vector allowing overexpression of Mrx6-myc from the ADH1 promoter. Cells were grown in dropout synthetic media with dextrose, lacking URA (SD-ura). PGK1 was used as a loading control. (F) qPCR analysis of mtDNA copy number in cells overexpressing Mrx6-myc, shown in E ($n = 4$).

(Figure 2, E and F). Mrx6-myc was functional because it maintained mtDNA at WT levels when it was expressed as the only copy of the gene. Deletion of *MRX6* increases mtDNA copy number without compromising mitochondrial function, while conversely overexpression of Mrx6 does not affect mtDNA levels.

Deletion of *MRX6* increases mtDNA copy number without altering mitochondrial network length or morphology

To test whether deletion of *MRX6* causes abnormalities in mitochondrial volume or morphology, we visualized the mitochondrial network in Δ*mrx6* and WT cells by fluorescence microscopy with a mitochondria-targeted red fluorescent protein (mt-dsRed; Figure 3A). We did not detect any changes in mitochondrial morphology (Figure 3, B and C) or network length (Figure 3D) in Δ*mrx6* cells, demonstrating that elevated mtDNA levels in Δ*mrx6* cells were not a consequence of morphological alterations.

To determine the copy number of mtDNA in single cells, we used our recently developed mt-LacO-LacI system to visualize mtDNA by fluorescence microscopy. The system is based on an array of LacO repeats integrated into mtDNA, which can be bound by a mitochondria-targeted GFP-tagged LacI protein (Osman *et al.*, 2015). In contrast to our previous work, we applied structured illumination (SI) microscopy on fixed diploid cells to resolve mtDNA copies that are in close proximity to one another (Figure 3A). We counted ~28 mtDNA copies in WT diploid cells, which is in good agreement with 33 (±6) mtDNA copies, determined by qPCR (Figure 2A), indicating that the microscopic analysis resolved single mtDNA copies in the majority of cases for WT cells. Given that cells used in this experiment were not synchronized and were going through different stages of the cell cycle, resulting in differences in cell size and mitochondrial volume, we compared mtDNA copy number normalized to mitochondrial network length. Deletion of *MRX6* increased the number of mtDNA copies normalized to mitochondrial network length 1.3-fold (Figure 3E; WT = 1.16, Δ*mrx6* = 1.54 mtDNA copies/μm network length). A 1.3-fold increase is smaller than what we obtained with qPCR (Figure 2A). We attribute the difference between microscopy and qPCR analysis to the fact that even with SI microscopy, we did not resolve

mtDNA copies that were close to one another (such as replicating mtDNA copies).

Next, we compared the distances between mtDNA copies in the three-dimensional mitochondrial network. Consistent with the increased number of nucleoids within the same length of mitochondrial network, the mean distances between mtDNA copies were 692 and 872 nm for Δ*mrx6* and WT cells, respectively ($p < 0.001$; Figure 3F). However, upon more detailed examination, we found that this difference was largely due to a closer apposition of a subset of mtDNA copies in the smaller distance range, while mtDNA copies further apart maintained their distribution as in WT cells. This bias is quantified in Figure 3G, which shows that mtDNA distances in the range 0.5–1.0 µm were disenriched in the mutant cells as compared with WT cells (Figure 3G, blue box), whereas mtDNA distances below 0.5 µm were enriched (Figure 3G, yellow box). These nonlinear alterations in the placement of mtDNA copies with respect to each other in Δ*mrx6* cells are in line with the observation that the overall mitochondrial network length is not altered in the mutant.

We next stained fixed diploid cells with DAPI (4′,6-diamidino-2-phenylindole) and analyzed them by SI microscopy (Figure 4A). In contrast to the LacO/LacI system shown above, DAPI stains mtDNA in its entirety, rather than just demarking a single locus on it. DAPI staining in WT cells revealed distinct punctate structures known as nucleoids (Meeusen and Nunnari, 2003). While Δ*mrx6* cells showed the same number of nucleoids, the average volume of nucleoids was enlarged ~2.2-fold in comparison with WT cells (Figure 4, B and C). We verified this finding using an anti-DNA antibody (Supplemental Figure 3) to ascertain that it was indeed DNA and not other DAPI-stained macromolecules, such as RNA, that gave rise to the increased volume. Notably, nucleoids in Δ*mrx6* cells displayed an oblong shape: their lengths, when traced along the mitochondrial network, were significantly increased (mean lengths of nucleoids were 630 and 430 nm for Δ*mrx6* and WT cells, respectively; $p < 0.001$; Supplemental Figure 3, A and B). Taken together, these data show that deletion of *MRX6* increases mtDNA copy number without affecting mitochondrial network length or shape, but alters the spatial organization and shape of nucleoids.

Mrx6 is a member of the PET20 domain–containing protein family

Interestingly, inspection of the Mrx6 sequence revealed the presence of a PET20 domain of uncharacterized structure and function, which in *S. cerevisiae* is found in two other mitochondrial proteins, Sue1 and Pet20 (Figure 5A). In addition to the PET20 domain, Mrx6 has a unique C-terminal extension that distinguishes it from the rest of the PET20 domain–containing proteins (Supplemental Figure 4). To assess whether other PET20 domain–containing proteins are important for maintaining mtDNA levels, we deleted the genes encoding these proteins in different combinations and quantified the change of mtDNA levels by qPCR. In line with the colony blots from the initial screen, single deletions of *PET20* or *SUE1* did not alter mtDNA levels significantly. Additionally, no further increase in mtDNA levels as compared with those for Δ*mrx6* cells was observed in Δ*mrx6* Δ*pet20*, Δ*mrx6* Δ*sue1*, and Δ*mrx6* Δ*pet20* Δ*sue1* double and triple mutant strains (Figure 5B). Thus, neither maintenance of normal mtDNA levels nor increase in mtDNA levels in Δ*mrx6* cells requires Pet20 or Sue1.

Mrx6 forms foci in mitochondria and colocalizes with mtDNA

Mrx6 has a predicted mitochondrial-targeting sequence, but to date its localization has not been determined experimentally. We constructed a yeast strain in which we genomically tagged Mrx6 in its endogenous locus with the fluorescent protein mNeonGreen (Mrx6-Neon) to determine its localization by fluorescence microscopy. Cells expressing Mrx6-Neon displayed mtDNA levels indistinguishable from those in WT cells, indicating that protein function was preserved in the tagged Mrx6 variant (Supplemental Figure 5A). In agreement with its predicted mitochondrial localization, Mrx6-Neon colocalized with mitochondrial matrix-targeted blue fluorescent protein (mtTagBFP; Figure 6A). Interestingly and in contrast to mtTagBFP, Mrx6-Neon formed discrete punctate structures that were nonuniformly distributed along the mitochondrial network.

The punctate localization of Mrx6-Neon was reminiscent of the distribution of mtDNA in the nucleoids in the mitochondrial network. Thus, we next tested whether Mrx6-Neon colocalizes with mtDNA. We stained Mrx6-Neon–expressing cells with DAPI and determined Mrx6-Neon and mtDNA localization. These analyses revealed that a fraction of Mrx6-Neon puncta colocalized with the DAPI signal (Figure 6B; arrow), whereas others did not (Figure 6B; asterisk). We quantitatively assessed the proportion of the Mrx6-Neon signal that colocalized with DAPI and vice versa by determining the Manders colocalization coefficient (MCC) between intensity profiles of the two fluorescent signals along the mitochondrial network (Figure 6C and Supplemental Figure 5B). The MCC values showed a broad distribution, yet the majority of cells showed ~60% overlap between the two wavelengths, confirming our initial observation of partial colocalization between Mrx6 and mtDNA (Figure 6D). Pearson's correlation coefficient (PCC) analysis further supported colocalization (Figure 6E). To validate these conclusions, we evaluated the significance of the measured MCC and PCC values by comparing our results with a control data set. This data set consisted of the same intensity profiles, in which one of the two color channels was randomized (Supplemental Figure 5C). The control MCC and PCC values were consistently lower and showed a distribution significantly different from that of the measured data (Figure 6, D and E, and Supplemental Figure 5D; $p < 0.001$). Additionally, comparing the measured MCC and PCC values to a simulated data set in which one of the two channels was shifted against the respective other channel, rather than randomized, further validated these results.

Given that only ~60% of the Mrx6-Neon puncta colocalized with nucleoids, we asked whether Mrx6 might still forms punctate structures in the absence of mtDNA. Mrx6-Neon was still observed in puncta in mitochondria of mtDNA-lacking cells (rho^0; Figure 6F). Taken together, these data show that Mrx6 localizes to mitochondria and forms puncta that distribute throughout the mitochondrial matrix and partially colocalize with mtDNA. However, the presence of mtDNA is not necessary for the formation of Mrx6 puncta.

Mrx6 forms a complex with Pet20, Mam33, and Pim1

Next, we aimed to identify interaction partners of Mrx6 to begin getting a molecular understanding of how Mrx6 affects mtDNA levels. To this end, we immunoprecipitated functional C-terminally Flag-tagged Mrx6 (Mrx6-Flag, Supplemental Figure 6) and identified interacting proteins by mass spectrometry (MS). The proteins Pim1, Mam33, and, to our surprise, Pet20 copurified with Mrx6-Flag but were absent in the eluate fraction of control immunoprecipitations from cells that only expressed untagged Mrx6 (Figure 7, A and B).

Pim1 is a highly conserved ATP-dependent mitochondrial Lon protease (Venkatesh *et al.*, 2012), and Mam33 is a specific translational activator of Cox1 mRNA (Roloff and Henry, 2015). We next asked whether, reciprocally, we could copurify these components by pulling down C-terminally Flag-tagged Pet20 (Pet20-Flag).

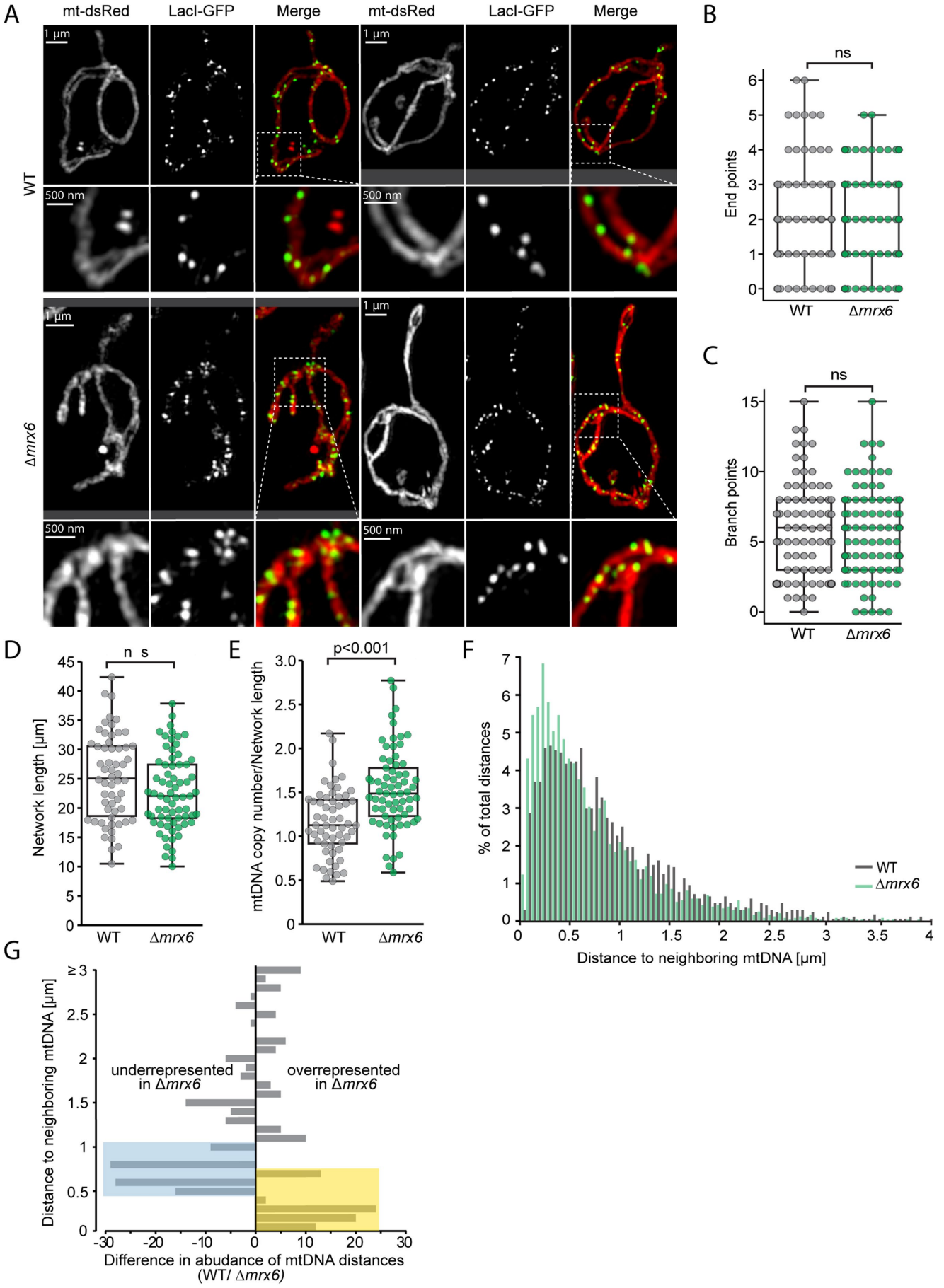
A
mt-dsRed
LacI-GFP
Merge
mt-dsRed
LacI-GFP
Merge
WT
Δmrx6
1 µm
500 nm
B
ns
End points
WT
Δmrx6
C
ns
Branch points
WT
Δmrx6
D
n s
Network length [µm]
WT
Δmrx6
E
p<0.001
mtDNA copy number/Network length
WT
Δmrx6
F
% of total distances
WT
Δmrx6
Distance to neighboring mtDNA [µm]
G
Distance to neighboring mtDNA [µm]
underrepresented in Δmrx6
overrepresented in Δmrx6
Difference in abudance of mtDNA distances (WT/ Δmrx6)

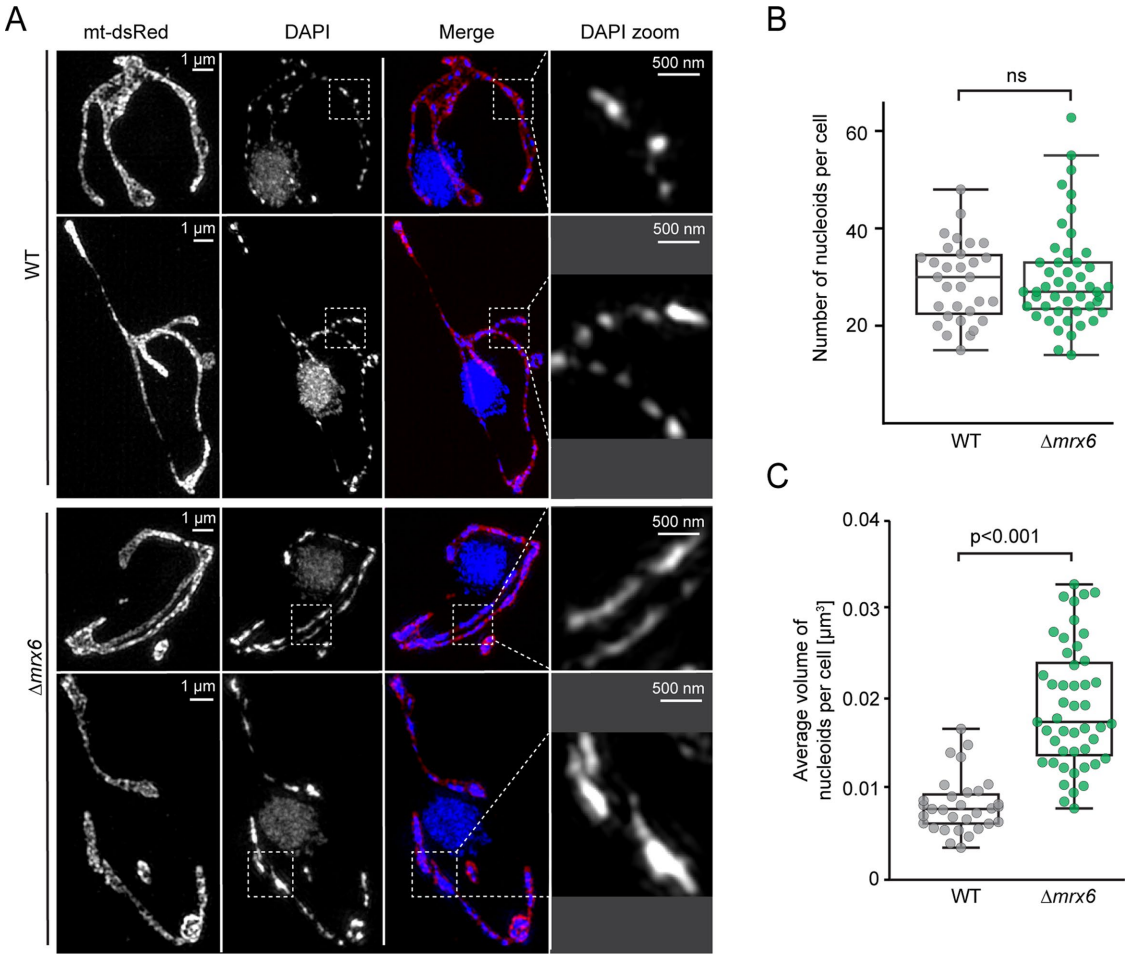

FIGURE 4: Δ*mrx6* cells display elongated nucleoids. (A) Z-projections of SI microscopic images of paraformaldehyde and methanol-fixed diploid cells that were stained with DAPI. Mitochondria were visualized by mt-dsRED. Cells were grown in SD-ura-trp. (B) Number and (C) average volume of nucleoids stained with DAPI in WT and Δ*mrx6* cells. Analysis was performed on three-dimensional images (31 cells for WT, 47 cells for Δ*mrx6*).

Strikingly, Mrx6, Pim1, and Mam33 copurified with Pet20-Flag, thus revealing an interaction network between these four proteins (Figure 7C). We further examined the interaction hierarchy of these proteins by pulling down Mrx6-Flag from extracts of Δ*pet20* cells. The results showed that Pet20 was dispensable for the interaction between Mrx6-Pim1 and Mrx6-Mam33 (Figure 7B). In contrast, upon Pet20-Flag pull down from Δ*mrx6* lysates, Pim1-Pet20 and Mam33-Pet20 interactions were drastically reduced and not detected, respectively, suggesting that Mrx6 bridges Pim1, Mam33, and Pet20 (Figure 7C).

Because two proteins of the PET20 domain protein family, Mrx6 and Pet20, are found in a protein interaction network together with Pim1 and Mam33, we asked whether the third member of the PET20-domain protein family, Sue1, would show a similar protein interaction profile. To this end, we immunoprecipitated C-terminally Flag-tagged Sue1 (Sue1-Flag). In agreement with the Mrx6-Flag

FIGURE 3: Deletion of *MRX6* increases mtDNA copy number without altering mitochondrial network length and morphology. (A) Z-projections of SI microscopic images of paraformaldehyde-fixed diploid WT and Δ*mrx6* cells. Mitochondria were visualized by mitochondria-targeted dsRed protein (mt-dsRed). LacI-GFP marks mtDNA. Cells were grown in SD-ura-trp. (B–E) Number of end points (B), branch points (C), length of mitochondrial network (D), and mtDNA copy number normalized to mitochondrial network length (E) in WT and Δ*mrx6* cells. Analysis was performed on three-dimensional images (58 cells for WT, 69 cells for Δ*mrx6*). (F) Histogram showing distribution of distances between neighboring mtDNA copies in WT and Δ*mrx6* cells in three-dimensional images. Means of distance between mtDNA copies are 692 and 872 nm for Δ*mrx6* and WT cells, respectively ($p < 0.001$). (G) Histogram depicting the differences in the abundance of distances between neighboring mtDNA copies (binning range 0.1 µm) between the observed WT distribution ($n = 1677$) and a remodeled Δ*mrx6* distribution. In the remodeled Δ*mrx6* distribution all determined distances in mutant cells ($n = 1677$) were multiplied by a factor of ~1.28 assuming that distances would be only shifted linearly to closer distances in Δ*mrx6* cells than in WT. Numbers of neighboring mtDNA copies in each binned distance range in the remodeled Δ*mrx6* distribution were replaced by the respective amounts determined for the WT distribution. The distance range from 0 to 0.7 µm that is overrepresented in the remodeled Δ*mrx6* distribution is highlighted in yellow; the one underrepresented between 0.5 and 1 µm is highlighted in blue. The remodeled Δ*mrx6* distribution is significantly different from the WT distribution ($\chi^2 = 52.67$, $df = 29$, $p < 0.005$).

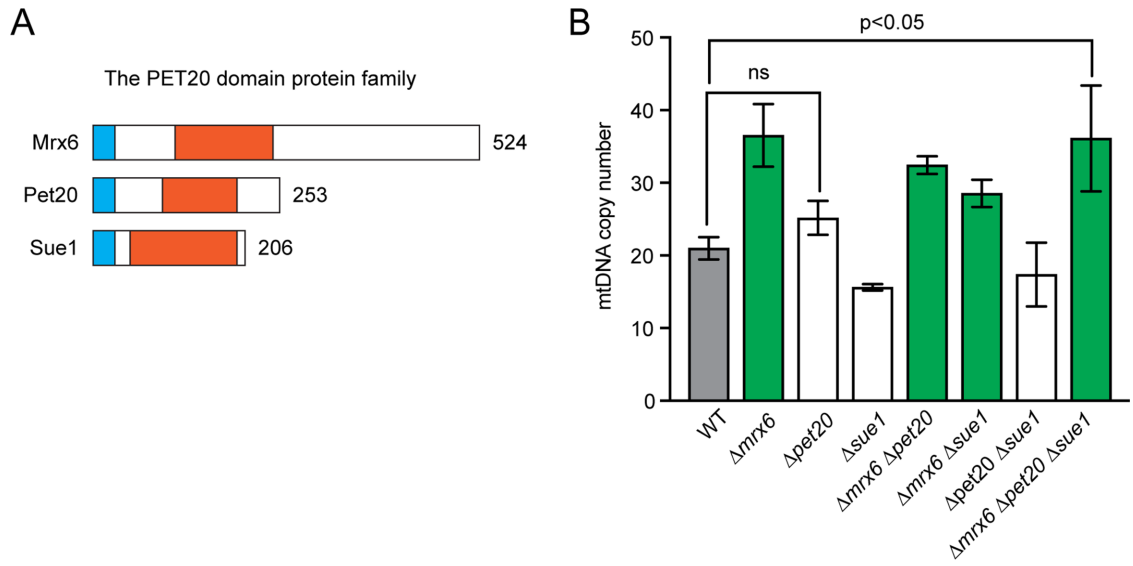

FIGURE 5: Mrx6 is a member of the PET20 domain–containing protein family. (A) Domain architecture of Mrx6 and other PET20 domain–containing proteins. Blue indicates mitochondrial targeting sequences. Orange represents PET20 domain. (B) Analysis of mtDNA copy number of single-, double-, and triple-deletion mutants of *MRX6, PET20*, and *SUE1*, measured by qPCR. Error bars are SD ($n = 2$). Cells were grown in YPD.

and Pet20-Flag pull downs, which did not identify Sue1, neither Mrx6 nor Pet20 coimmunoprecipitated with Sue1-Flag. However, this experiment revealed that Pim1 also interacts with Sue1 (Figure 7D). Thus, Pim1 is a common interaction partner of all three PET20 domain–containing proteins.

Taken together, these results show that Mrx6, Pet20, Pim1, and Mam33 are part of a physical interaction network in which Mrx6 is crucial for the complex's architecture, whereas Pet20 is dispensable. In addition, our results support the conclusion that Sue1 forms a separate complex with Pim1, which does not include Mrx6 or Pet20.

Mrx6 partially colocalizes with Pet20 and Pim1

As Mrx6 and Pet20 are part of an interaction network, we next examined the spatial association between them in single cells. To this end, we engineered a yeast strain expressing Mrx6-Neon and C-terminally mRuby-tagged Pet20 (Pet20-Ruby) and performed live-cell microscopy.

Pet20-Ruby showed discrete punctate structures along the mitochondrial network similar to those for Mrx6 (Figure 8A). Surprisingly, we observed only partial colocalization between Mrx6 and Pet20, in which only some of the Mrx6-Neon puncta colocalized with Pet20-Ruby (Figure 8A, arrow), and vice versa. MCC values showed ~50% overlap between Mrx6-Neon and Pet20-Ruby signals (Figure 8B and Supplemental Figure 7A; $p < 0.001$), and PCC analysis confirmed their colocalization (Figure 8C; $p < 0.001$).

We next tested whether Mrx6 would display a similar partial colocalization with Pim1, a notion suggested by our finding that Pim1 forms a separate complex with Sue1 that lacks Mrx6 or Pet20 (Figure 7D). Hence, we analyzed the association between Mrx6 and Pim1 using a yeast strain expressing Mrx6-Neon and C-terminally mRuby-tagged Pim1 (Pim1-Ruby), which preserves protein function (Supplemental Figure 7B). We observed partial colocalization between Mrx6 and Pim1 (Figure 8D). MCC values showed ~50% overlap between Mrx6-Neon and Pim1-Ruby signals (Figure 8E and Supplemental Figure 7C; $p < 0.001$), and PCC analysis further supported their colocalization (Figure 8F; $p < 0.001$). Taken together, these data indicate that Mrx6 partially colocalizes with Pet20 and Pim1, suggesting that they form subcomplexes along the mitochondrial network.

The Mrx6 complex colocalizes with mtDNA

We next tested whether colocalization of Mrx6 with Pet20 and Pim1 may occur preferentially in regions close to mtDNA. To this end, we performed triple labeling experiments in which we stained mtDNA with DAPI in cells expressing Mrx6-Neon and Pet20-Ruby. This experiment revealed instances of colocalization between Mrx6-Neon, Pet20-Ruby, and mtDNA (Figure 9A). The complexity of images displaying three colors in the confined space of mitochondria necessitated careful quantification of the degree of colocalization. To this end, we binned regions of the Mrx6-Neon and Pet20-Ruby intensity profiles where 1) both proteins colocalized, 2) only Mrx6-Neon but not Pet20-Ruby localized, and 3) only Pet20-Ruby but not Mrx6-Neon localized. We then asked whether these regions would colocalize differentially with mtDNA. Determination of the MCC values revealed that in Bin1 (Mrx6-Pet20), on the average, 77% of the regions colocalized with DAPI (Figure 9B and Supplemental Figure 8A). In contrast, in Bin 2 (Mrx6 alone) or Bin 3 (Pet20 alone) only 56% or 42% of the regions, respectively, colocalized with DAPI, which was significantly different from the result for Bin 1 ($p < 0.001$; Figure 9B and Supplemental Figure 8A). As a control, we generated a data set by randomizing the DAPI intensity profile against the Mrx6 and Pet20 profiles and recalculated the MCC values. Strikingly, the proportion of the Mrx6-Pet20 signal colocalizing with the DAPI signal was reduced to 44% (Figure 9C and Supplemental Figure 8B), matching the colocalization with mtDNA observed for Mrx6 alone (45%; Bin 1 – Bin 2, $p = 0.78$; Figure 9C) or Pet20 alone (44%; Bin 1 – Bin 3, $p = 0.79$; Supplemental Figure 8B). These results suggest that Mrx6-Pet20 colocalization occurs preferentially in regions close to mtDNA rather than areas that are devoid of mtDNA.

In an analogous set of experiments, we examined the colocalization between Mrx6-Neon, Pim1-Ruby, and mtDNA (Figure 9D). The MCC values revealed that on the average 65% of the areas in which Mrx6-Neon and Pim1-Ruby were found together colocalized with

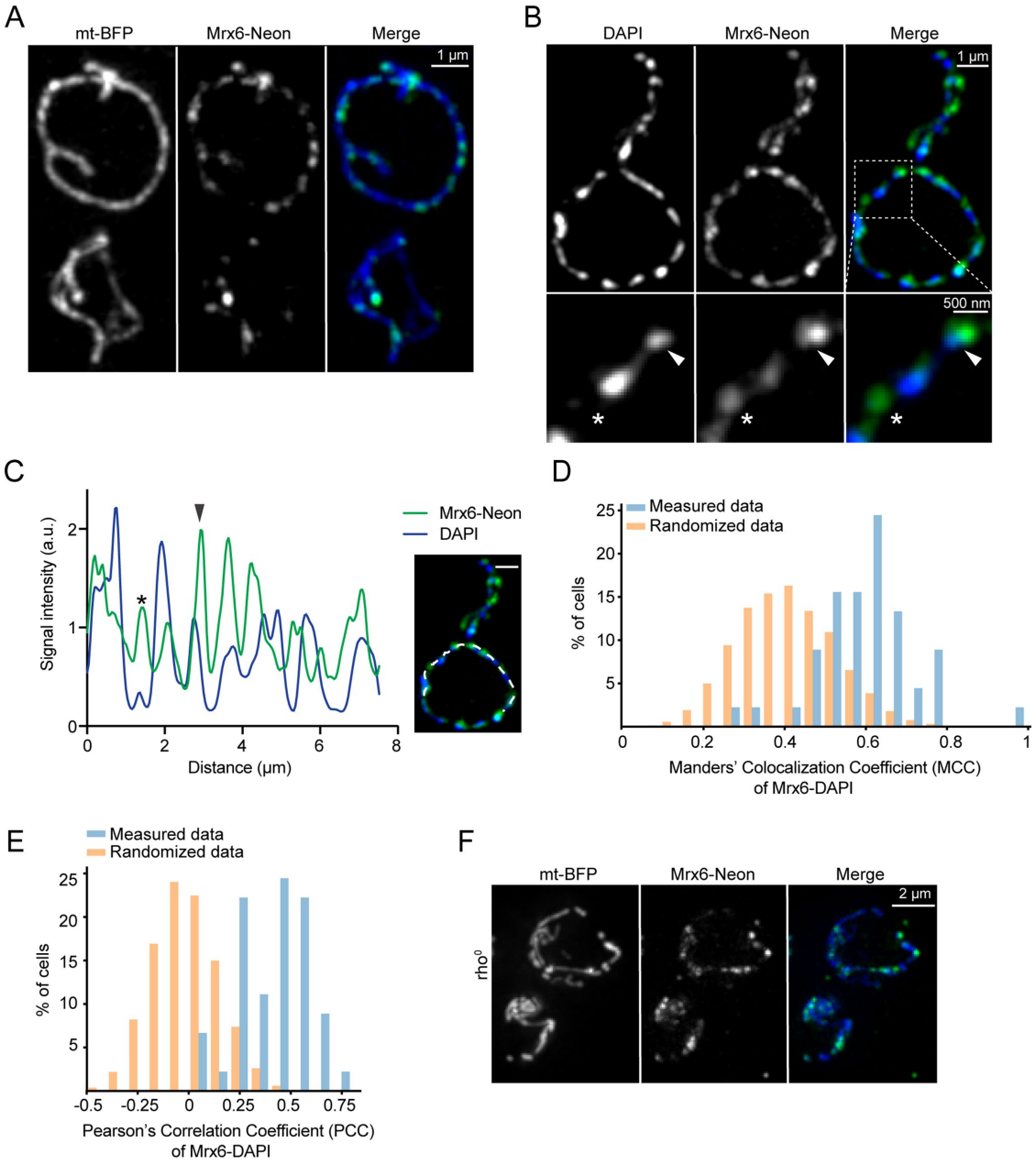

FIGURE 6: Mrx6 forms foci in mitochondria and colocalizes with mtDNA. (A) Z-projection of microscopic images of a live cell expressing Mrx6-Neon. Mitochondria were visualized by mt-BFP. Mrx6-Neon (green), mt-BFP (blue) in the merged image. Cells were grown in SD-ura-trp. (B) Z-projections of microscopic images of a live cell expressing Mrx6-Neon (green). mtDNA was stained with DAPI (blue). Arrowhead shows colocalization of Mrx6-Neon and DAPI; asterisk marks noncolocalization. Cells were grown in SD-trp. (C) Linescan analysis of mitochondrial network for the cell shown in B. (D) Distribution of MCC calculated for colocalization of Mrx6-Neon with DAPI in 47 cells (mean = 0.60) or in the same linescans where the DAPI signal was randomized (mean = 0.42, $p < 0.001$). (E) Distribution of PCC determined for Mrx6-Neon and DAPI line cans in measured data ($n = 47$ cells, mean = 0.40) and in randomized data (mean = 0, $p < 0.001$). (F) Z-projection of microscopic images of a live cell that lacks mtDNA but expresses Mrx6-Neon (green). Mitochondria were visualized by mt-BFP (blue). Cells were grown in SD-ura.

the DAPI signal (Figure 9E and Supplemental Figure 8C); whereas only 46% of the Mrx6 signal ($p < 0.001$; Figure 9E) and 36% of the Pim1 signal colocalized with the DAPI signal when they were alone ($p < 0.001$; Supplemental Figure 8C). Moreover, the percentage of the Mrx6-Pim1 signal colocalizing with the randomized DAPI signal decreased to 38% (Figure 9F and Supplemental Figure 8D), closely matching the values for Mrx6 alone (37%; $p = 0.49$; Figure 9F) and Pim1 alone (38%; $p = 0.29$; Supplemental Figure 8D). These data indicate that similarly to that of Mrx6-Pet20, Mrx6-Pim1 colocalization occurs in areas close to mtDNA. Taken together, our data suggest that Mrx6 associated with Pet20 or Pim1 preferentially colocalizes with mtDNA, whereas the individual components—or yet-to-be-defined partially assembled subcomplexes—are mostly found in the areas devoid of mtDNA.

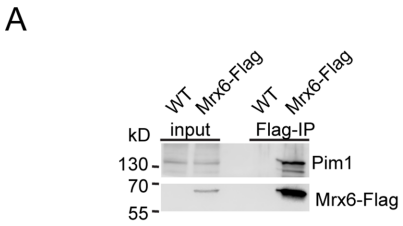

B

Mrx6-Flag immunoprecipitation

Total spectral count	WT	Mrx6-Flag	Δpet20 Mrx6-Flag	Δsue1 Mrx6-Flag
Pim1	0	555	354	434
Mrx6	0	151	98	114
Pet20	0	44	0	44
Mam33	0	66	44	42

C

Pet20-Flag immunoprecipitation

Total spectral count	WT	Pet20-Flag	Δmrx6 Pet20-Flag	Δsue1 Pet20-Flag
Pim1	0	391	6	484
Mrx6	0	67	0	86
Pet20	0	50	21	67
Mam33	0	39	0	46

D

Sue1-Flag immunoprecipitation

Total spectral count	WT	Sue1-Flag	Δpet20 Sue1-Flag	Δmrx6 Sue1-Flag
Pim1	0	59	55	41
Mrx6	0	0	0	0
Pet20	0	0	0	0
Mam33	0	0	0	0
Sue1	0	3	4	3

FIGURE 7: Mrx6 binds to Pet20, Pim1, and Mam33. (A) Western blot analyses of an anti-Flag immunoprecipitation experiment from cells expressing Mrx6-Flag or Mrx6 (WT). Membranes were probed with antibodies against Pim1 (top) and the Flag epitope (bottom). Cells were grown in YPD. (B) Interaction partners of Mrx6-Flag in cells expressing Mrx6-Flag but lacking Pet20 or Sue1, identified by anti-Flag immunoprecipitation and mass spectrometry analysis. The numbers represent total spectral count. Cells were grown in YPD. (C) Interaction partners of Pet20-Flag in cells expressing Pet20-Flag but lacking Mrx6 or Sue1. Same as above. (D) Interaction partners of Sue1-Flag in cells expressing Sue1-Flag but lacking Mrx6 or Pet20. Same as above.

Depletion of Pim1 increases mtDNA levels

Our biochemical and microscopic analyses suggest that Mrx6 may determine mtDNA levels via its interaction with Pim1. To test this model, we examined mtDNA levels in cells overexpressing or lacking Pim1 by qPCR. Overexpression of Pim1 in WT and Δ*mrx6* cells reduced mtDNA copy number (Supplemental Figure 10A), supporting a putative role of Mrx6 as a regulatory component conferring substrate specificity to Pim1. However, when *PIM1* was deleted, mtDNA copy numbers varied widely in different Δ*pim1* and Δ*pim1*Δ*mrx6* clones, preventing an unequivocal interpretation (Supplemental Figure 10B). These inconsistent results are likely explained by the dysregulated accumulation of the many Pim1 substrates (Major *et al.*, 2006; Bayot *et al.*, 2010), leading pleiotropically to mitochondrial dysfunction.

To mitigate such pleiotropic effects, we integrated a construct facilitating estradiol-dependent expression of Pim1 into WT yeast strains and subsequently generated endogenous deletions of either *PIM1* (Δ*pim1 Pestr-PIM1*) or *MRX6* and *PIM1* (Δ*mrx6* Δ*pim1 Pestr-PIM1*). Pim1 expression was maintained throughout strain generation by growing cells in the presence of estradiol. Estradiol concentrations of 25 nM were sufficient to restore respiratory growth in Δ*pim1* background under the experimental conditions at 30°C (Figure 10C) and also resulted in low expression levels that allowed fast Pim1 depletion upon estradiol removal (Figure 10B).

We acutely depleted Pim1 by shifting cells to a medium lacking estradiol and determined mtDNA levels over the course of 20 h (Figure 10, A and B). In line with the low expression level of Pim1 at the start of the experiment, mtDNA levels were increased ~1.3-fold in Δ*pim1 Pestr-PIM1* cells from those in WT. When Pim1 was depleted, 12 h after removal of estradiol, mtDNA levels were increased 1.8-fold in Δ*pim1 Pestr-PIM1* cells (Figure 10A). Similarly increased levels were detected in the Δ*mrx6* Δ*pim1 Pestr-PIM1* double mutant, even at the start of the experiment, when Pim1 was still present. Strikingly, over the time course, mtDNA levels did not increase further in cells lacking both proteins. This strongly supports a model in which Mrx6 acts via Pim1 to maintain WT mtDNA copy numbers.

DISCUSSION

We identified new cellular components that modulate mtDNA levels in yeast using a forward genetic screen. We examined mtDNA levels in the 5148 mutants of a yeast deletion library and found that ~2% of these mutants had elevated levels of mtDNA relative to WT. Remarkably, the vast majority of these mutants (~85%) displayed less than a 2.5-fold increase in mtDNA levels, suggesting that a single gene deletion is not sufficient to alter mtDNA levels more drastically. This finding suggests that mtDNA copy number is under stringent regulation, which may be explained by a multilayered system that involves a combination of various components, including factors regulating mtDNA replication and/or stability. One such layer that affects mtDNA levels is cell size, as the majority of our hits with elevated mtDNA copy number displayed increased cell size. This finding supports the notion that mtDNA copy number scales with mitochondrial network length, which in turn scales with cell volume (Rafelski *et al.*, 2012; Osman *et al.*, 2015). Therefore, in contrast to the nuclear genome, mtDNA copy number appears not to be determined on a "per cell" basis, but rather on a "per cell volume" basis. It remains an exciting task for future studies to unravel the molecular basis underlying the coordination between mitochondrial volume, mtDNA copy number, and cell size.

For the nine mutants that displayed elevated mtDNA levels and unaltered cell size, we examined the role of Mrx6 in maintenance of mtDNA levels. Mrx6 has been previously identified in a complex with the mitochondrial ribosome and named "Mitochondria oRganization of gene eXpression 6" (Kehrein *et al.*, 2015). However, to date the function of Mrx6 has remained obscure. Based on the following observations, Mrx6 appears directly linked to mtDNA copy-number regulation: 1) Δ*mrx6* cells do not display a growth defect on a nonfermentable carbon source, ruling out the conclusion that mtDNA levels are elevated due to a compensatory feedback

loop that responds to a defective respiratory chain; 2) Δ*mrx6* cells respond to a change in carbon source and display elevated mtDNA levels relative to WT on both fermentable and nonfermentable carbon sources, excluding the possibility that Δ*mrx6* cells are defective in glucose repression (Ulery *et al.*, 1994); 3) Δ*mrx6* cells do not exhibit any changes in mitochondrial network length or morphology, which excludes the possibility that increased mtDNA levels are caused by compromised mitochondrial structure. Thus, elevated mtDNA levels in Δ*mrx6* cells are not simply secondary effects caused by mitochondrial or cellular dysfunction.

Interestingly, deletion of *MRX6* resulted in elongated nucleoids. One plausible explanation for this phenotype is that newly replicated copies of mtDNA in Δ*mrx6* cells remain at least partially associated with parental mtDNA, resulting in bigger and misshapen nucleoids. The oblong shape of nucleoids is reminiscent of the proposed nucleoid division defects in *HSP60* mutants (Kaufman *et al.*, 2003). In line with this notion, we observed clustering of mtDNA copies when mtDNA was visualized with the mt-LacO-LacI system by structured illumination microscopy, which allowed detection and analysis of the spatial distribution of individual mtDNA copies. Alternatively, deletion of *MRX6* could change the packaging of nucleoids, resulting in less compact and elongated nucleoids, which could alter mtDNA levels, perhaps by providing more access to the origins of replication.

Mrx6 contains a PET20 domain of uncharacterized structure and function that is conserved in fungi, including distant species such as *Schizosaccharomyces pombe*. Two other proteins in *S. cerevisiae*, Pet20 and Sue1, also belong to the PET20 protein family and localize to mitochondria (Wei and Sherman, 2004; Polevoda *et al.*, 2006). We see no alterations in mtDNA levels upon deletion of *PET20* or *SUE1*, alone or in combination, suggesting that both genes either are required in other molecular contexts or only affect mtDNA copy number regulation to minor extents.

Our protein-interaction studies revealed a complex network composed of the PET20 domain–containing proteins and the proteins Mam33 and Pim1. Mam33 was identified as an Mrx6 interaction partner and is a specific translational activator of Cox1 mRNA (Roloff and Henry, 2015). The physiological role of the interaction between Mrx6 and Mam33 is currently unknown. However, the interaction points to regulatory coordination between translation and mtDNA copy number, which remains to be clarified in future studies. Interestingly, such coordination has recently been proposed for SLIMP, a specialized mitochondrial aminoacyl t-RNA synthetase paralogue, which affects mtDNA levels and interacts with the Pim1 Lon homologue in arthropods (Picchioni *et al.*, 2019).

Remarkably, Mrx6, Pet20, and Sue1 are found in protein complexes that contain the conserved mitochondrial Lon protease Pim1, which reveals a strong link between the PET20 domain–containing proteins and the mitochondrial-protein quality-control system. The finding that copurification of Pim1 with Pet20 depends on Mrx6 and that Mrx6 copurifies with Pet20 suggests that Pim1, Mrx6, and Pet20 may be part of the same complex. In contrast, Sue1 forms an alternate complex with Pim1.

We consider it an attractive possibility that PET20 domain–containing proteins serve as substrate specificity factors for Pim1. In agreement, Sue1 is required for degradation of labile forms of cytochrome *c* (Wei and Sherman, 2004), suggesting that Sue1-Pim1–dependent proteolysis could play a role in degradation of altered forms of cytochrome *c* (albeit it remains a paradox how misfolded cytochrome *c* would venture into the mitochondrial matrix space to meet its fate or, vice versa, how Sue1-Pim1 might gain access to the intermembrane space to hunt for misfolded cytochrome *c*). By analogy, Mrx6 may be important for Pim1-dependent degradation of proteins regulating mtDNA copy number. In support of this idea, we found that acute depletion of Pim1 results in elevated mtDNA levels matching those observed in Δ*mrx6* cells. However, depletion of Pim1 in Δ*mrx6* cells did not lead to a further increase in mtDNA copy number, thus revealing an epistatic relationship between Mrx6 and Pim1. These observations strongly support our hypothesis that Mrx6 acts through Pim1 to regulate mtDNA levels.

Although we consider it an attractive hypothesis, we currently have no direct evidence that mtDNA copy number is affected through the proteolytic activity of Pim1. However, in support of this notion, Pim1 has been shown to degrade multiple proteins involved in mtDNA metabolism (Bayot *et al.*, 2010). For example, Abf2, a mtDNA packaging protein required for mtDNA stablility, has been reported to be a substrate of Pim1 and changes in Abf2 protein levels alter mtDNA copy number (Zelenaya-Troitskaya *et al.*, 1998; Bayot *et al.*, 2010). Moreover, the orthologue of Abf2 in higher eukaryotes, TFAM, modulates mtDNA levels (Ekstrand *et al.*, 2004; Kanki *et al.*, 2004), and changes in Lon protease expression alter mtDNA copy number through degradation of TFAM (Matsushima *et al.*, 2010; Lu *et al.*, 2013). In our hands, however, in Δ*mrx6* cells' overall Abf2 protein levels did not change relative to WT cells, suggesting that the increased mtDNA phenotype in Δ*mrx6* cells relies on subtle local changes if Abf2 is an Mrx6-dependent Pim1 substrate (Supplemental Figure 10). Similarly, the human mitochondrial protease Lon degrades the DNA helicase Twinkle (Kunova *et al.*, 2017). Therefore, mtDNA copy number regulation by Mrx6-Pim1-dependent proteolysis might not be limited to a single substrate.

Pim1 colocalizes with nucleoids (Kunova *et al.*, 2017), and its human homologue binds to mtDNA, preferentially in the control region where mtDNA transcription and replication are initiated (Lu *et al.*, 2007). While our localization studies support an Mrx6-dependent link between Pim1 and mtDNA, our attempts to footprint the Pim1-Mrx6 complex on mtDNA by chromatin immunoprecipitation have been unsuccessful. Interestingly, we found Mrx6 complexes containing Pim1 and/or Pet20 in the close vicinity of mtDNA, whereas the fraction of Mrx6 not colocalizing Pim1 and/or Pet20 was found predominately in DNA-free areas.

In summary, we propose the model in Figure 11: Mrx6 in complex with Pim1, Pet20, and Mam33 localizes to mtDNA. Mrx6 then facilitates substrate recognition of Pim1 and degradation of factors that stimulate mtDNA replication. Accordingly, absence of Mrx6 would lead to an accumulation of such factors and in turn increase the number of mtDNA in the organelle.

Mitochondria evolved as endosymbionts from ancestral bacteria. In this light, it is exciting that Lon proteases are also involved in regulating replication of bacterial genomes. *Caulobacter crescentus* and *Escherichia coli* Lon proteases, for example, affect DNA replication by degrading a replication initiation factor and an inhibitor, respectively (Langklotz and Narberhaus, 2011; Jonas *et al.*, 2013). Therefore, our results identify a novel component in an evolutionarily conserved regulatory mechanism of mtDNA replication.

MATERIALS AND METHODS

Yeast strains and plasmids

The yeast strains used in this study are derived from W303 and are listed in Supplemental Table 2. Deletion of yeast genes was performed in diploid strains and C-terminal tagging of genes was done in haploid strains using homologous recombination as described previously (Janke *et al.*, 2004). Haploid cells were used for all experiments, except those shown in Figures 2A, 3, and 4, where diploids

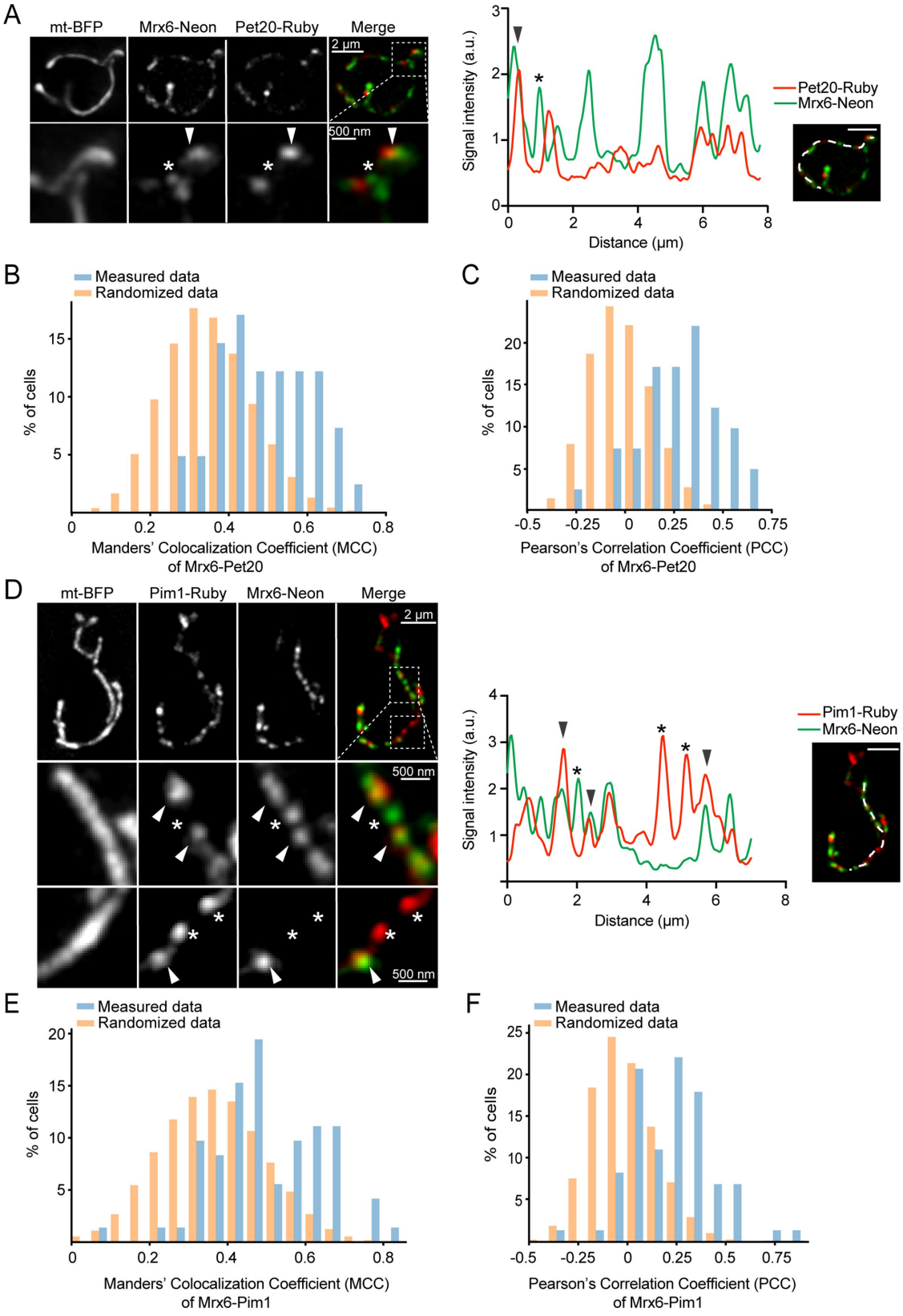

FIGURE 8: Mrx6 partially colocalizes with Pet20 and Pim1. (A) Z-projections of microscopic images of a live cell expressing Mrx6-Neon (green) and Pet20-Ruby (red). Linescan analysis of mitochondrial network is shown on the right. Arrowhead indicates colocalization of Mrx6-Neon and Pet20-Ruby; asterisk marks noncolocalization. Cells were grown in SD-ura-trp. (B) Distribution of MCC determined for colocalization of Mrx6-Neon with Pet20-Ruby in measured ($n = 41$ cells, mean = 0.50) and randomized data (mean = 0.36, $p < 0.001$). (C) Distribution of PCC between Mrx6-Neon and Pet20-Ruby in measured ($n = 41$ cells, mean = 0.28) and randomized data (mean = 0, $p < 0.001$). (D) Z-projections of

cells were used. Plasmids and oligonucleotides used in this study are listed in Supplemental Tables 3 and 4, respectively.

Colony blot hybridization

A previously described protocol (Kleinman, 1996) was followed with minor additions to optimize the protocol for fluorescent hybridization. Briefly, the mutants of the yeast deletion library were grown on glucose rich agar plates and transferred to nylon membranes (Bright Star-plus was used for the first and second screens, and Pall Biodyne A was used for the third screen) by incubating membranes on plates for 5 min, followed by gentle lifting. Membranes were air-dried for 5 min; placed, colony side up, on Whatman 3M papers that were soaked with reducing buffer (1 M sorbitol, 50 mM DTT, 20 mM EDTA, 10 mM NaAzide, 10 mM KF); and kept at RT (room temperature) for 20 min. Subsequently, membranes were transferred onto Whatman 3M papers that were soaked with lysis buffer (1 M sorbitol, 10 mM DTT, 20 mM EDTA, 10 mM Tris-HCl, pH 7.6, 10 mM NaAzide, 10 mM KF, 3 mg/ml zymolyase 20-T) and kept overnight in a closed container at 37°C. The next day, membranes were placed on Whatman 3M papers that were soaked with 0.5 M NaOH for 10 min. Membranes were air-dried for 5 min and neutralized by incubating on Whatman 3M papers saturated with 0.5 M Tris-HCl, pH 7.5/5X SSC (saline sodium citrate) for 5 min, two times, and transferred onto Whatman 3M papers saturated with TE pH 7.5/1X SSC (150 mM NaCl, 15 mM sodium citrate) for 5 min. Following neutralization, membranes were placed on Whatman 3M papers soaked with TE pH 7.5/1X SSC buffer with 0.2 mg/ml RNaseA (Sigma) and kept in a closed container for 2 h at 37°C. Subsequently, membranes were placed on Whatman 3M papers that were soaked with 100 mM Tris-HCl, pH 7.5/1X SSC for 5 min two times, air-dried, and baked at 65°C for 30 min, followed by cross-linking with 254-nm UV irradiation at 60 mJ/cm^2. Membranes were placed in hybridization bottles and washed two times with 5X SSC, 0.5% SDS, 10 mM EDTA for 15 min while rotating at 65°C. Membranes were rinsed with Proteinase K buffer (50 mM Tris HCl, pH 7.5, 10 mM EDTA, 1% SDS, 50 mM NaCl) and incubated in Proteinase K buffer containing 2 mg/ml Proteinase K (Invitrogen) for 2 h at 55°C. Membranes were rinsed with 5X SSC and washed with 3 M urea, 1% SDS at 55°C, three times for 10 min each. Membranes were further washed with 5X SSC two times for 15 min each and prehybridized for 2 h with hybridization buffer (50% formamide, 8% dextran sulfate, 2.5X SSC, 5 mM EDTA, 25 mM HEPES-KOH, pH 7, 3% SDS) at 42°C. Membranes were hybridized with fluorescently labeled probes (final concentration 100 ng/ml mtDNA-Cy3 probe mix and 100 ng/ml nuclear DNA-Cy5 probe mix) in hybridization buffer at 42°C overnight. The next day, membranes were washed with wash buffer (1X SSC, 1% SDS) three times for 10 min each at 65°C. Membranes were completely air-dried before being scanned with a Typhoon fluorescence scanner using Cy3 and Cy5 channels at normal sensitivity.

Preparation of probes for hybridization

Probes were prepared by PCR using Phusion DNA polymerase and different pairs of primers (Supplemental Table 4). Twelve different probes were pooled to detect nuclear DNA, and two different probes were pooled to detect mtDNA. PCR products were cleaned and concentrated with Zymo DNA Clean & Concentrator-5 and labeled with Mirus *Label* IT nucleic acid labeling kits using Cy3 or Cy5 dyes overnight according to the product manual. Labeled probes were EtOH-precipitated and stored at –30°C. Probes were boiled for 5 min before addition into hybridization buffer.

Quantification of colony blots

Scans of colony blots were quantified with ImageJ. The median signal intensity of each colony, for Cy3 and Cy5 channels, was determined after background subtraction using a rolling ball plug-in. Autofluorescence of yeast colonies was measured in both channels from a sample membrane that had not been incubated with probes. Autofluorescence of colonies correlated linearly with colony size, and thus we developed an algorithm that calculates autofluorescence for each mutant depending on its colony size. The hybridization signal for each colony was calculated by subtracting the estimated autofluorescence from the median signal intensity. However, later we found out that autofluorescence also correlates with respiratory capability, which explains why the mutants that lack mtDNA have mtDNA/nDNA ratios below zero after subtraction of colony autofluorescence. To calculate relative fold changes in mtDNA/nDNA ratios, mtDNA/nDNA ratios of all mutants except the ones that had lost mtDNA were averaged and used for normalization of each mutant mtDNA/nDNA ratio.

Cell growth and quantitative PCR

Prior to harvesting, yeast cells were grown in liquid media (YPD [yeast extract peptone dextrose], YPEG [yeast extract peptone ethanol gylcerol], or drop-out synthetic media) in log phase for 24 h at 30°C. In Figure 2C, cells were treated with 0.5 mM H_2O_2 in YPD for 1 h. In Figure 2D, cells were treated with DMSO (dimethyl sulfoxide) or FCCP (5 µg/ml) in YPD for 1 h. Genomic DNA (gDNA) was extracted using the Thermo Scientific Pierce Yeast DNA extraction rReagent or Zymo ZR-96 fungal/bacterial DNA kits. gDNA was subjected to qPCR using iQ-Syber Green Supermix (Bio-RAD) and primers specific for Cox1 and Act1 genes according to the manufacturer's manual (Supplemental Table 4). For absolute mtDNA copy number quantification, 1-kb fragments of Cox1 and Act1 genes were cloned into pUC19 plasmids and used as standards for copy number quantification. For statistical analysis of qPCR data, an unpaired *t* test was used for comparison of two groups and one-way analysis of variance was used for multiple comparisons, followed by Tukey's multiple comparison test in GraphPad Prism.

Flow cytometry

Yeast cells were grown overnight in liquid media (YPD) in 96-well polystyrene plates at 30°C and the next morning were diluted, regrown for ~4 doubling times, and harvested at OD_{600} = ~0.5–1. Yeast cultures were then transferred to 96-well microplates (Corning), diluted with YPD at a 1:5 ratio, and analyzed by a flow cytometer (LSR II, Beckton–Dickinson) and a high-throughput sampler (BD high-throughput sampler; Beckton–Dickinson) to inject samples into

microscopic images of a live cell expressing Mrx6-Neon (green) and Pim1-Ruby (red). Linescan analysis of mitochondrial network is shown on the right. Arrowhead indicates colocalization of Mrx6-Neon and Pim1-Ruby; asterisk marks noncolocalization. Cells were grown in SD-ura-trp. (E) Distribution of MCC determined for colocalization of Mrx6-Neon with Pim1-Ruby in measured (n = 69 cells, mean = 0.50) and randomized data (mean = 0.37, $p < 0.001$). (F) Distribution of PCC between Mrx6-Neon and Pim1-Ruby in measured (n = 69 cells, mean = 0.22) and randomized data (mean = 0, $p < 0.001$).

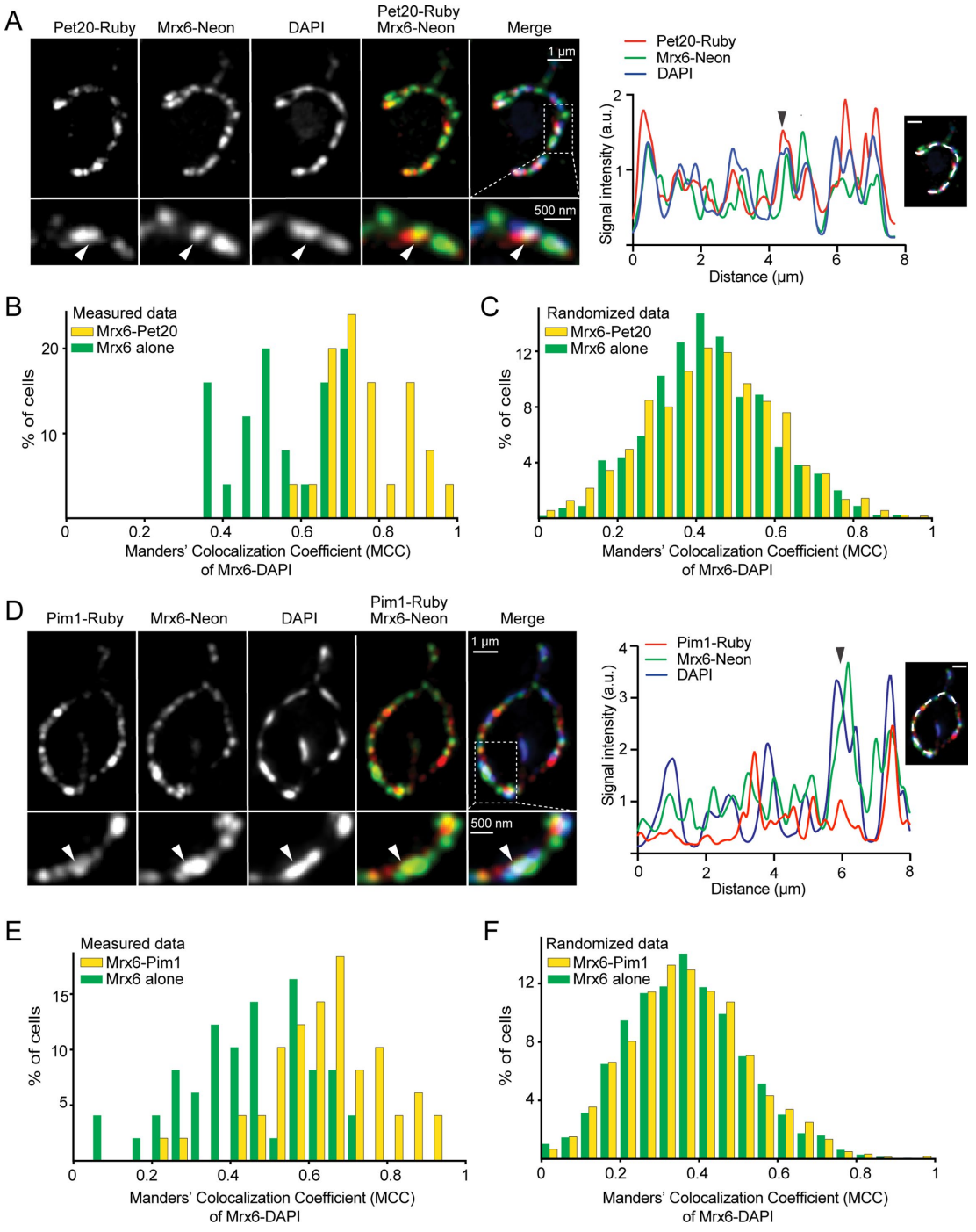

FIGURE 9: Mrx6 colocalizes with Pet20 and Pim1 in regions close to mtDNA. (A) Z-projections of microscopic images of a live cell expressing Mrx6-Neon and Pet20-Ruby. mtDNA was stained with DAPI. Mrx6-Neon (green), Pet20-Ruby (red), and DAPI (blue) in the merged images. Linescan analysis of mitochondrial network is shown on the right. Arrowhead indicates colocalization of Mrx6-Neon, Pet20-Ruby, and DAPI signal. Cells were grown in SD-trp. (B) Distribution of MCC determined for colocalization of Mrx6-Pet20 (Mrx6-Neon colocalizing with Pet20-Ruby) with DAPI signal ($n = 25$ cells, mean = 0.77) and Mrx6 alone (not colocalizing with Pet20-Ruby) with DAPI signal (mean = 0.56, $p < 0.001$). (C) Distribution of MCC determined for colocalization of Mrx6-Pet20 (Mrx6-Neon colocalizing with Pet20-Ruby) with randomized DAPI signal ($n = 25$ cells, mean = 0.44) and Mrx6-Neon alone (not colocalizing with Pet20-Ruby) with randomized DAPI signal (mean = 0.45, $p = 0.78$). (D) Z-projections of microscopic images of a live cell expressing Mrx6-Neon (green) and Pim1-Ruby (red). mtDNA was stained with DAPI (blue). Linescan analysis of mitochondrial network is shown on the right. Arrowhead indicates colocalization of Mrx6-Neon, Pim1-Ruby, and DAPI signal. Cells were grown in SD-trp. (E) Distribution of MCC determined for colocalization of Mrx6-Pim1 (Mrx6-Neon colocalizing with Pim1-Ruby) with DAPI signal ($n = 49$ cells, mean = 0.65) and Mrx6 alone (not colocalizing with Pim1-Ruby) with DAPI signal (mean = 0.46, $p < 0.001$). (F) Distribution of MCC determined for colocalization of Mrx6-Pim1 (Mrx6-Neon colocalizing with Pim1-Ruby) with randomized DAPI signal ($n = 49$ cells, mean = 0.38) and Mrx6 alone (not colocalizing with Pim1-Ruby) with randomized DAPI signal (mean = 0.37, $p = 0.49$).

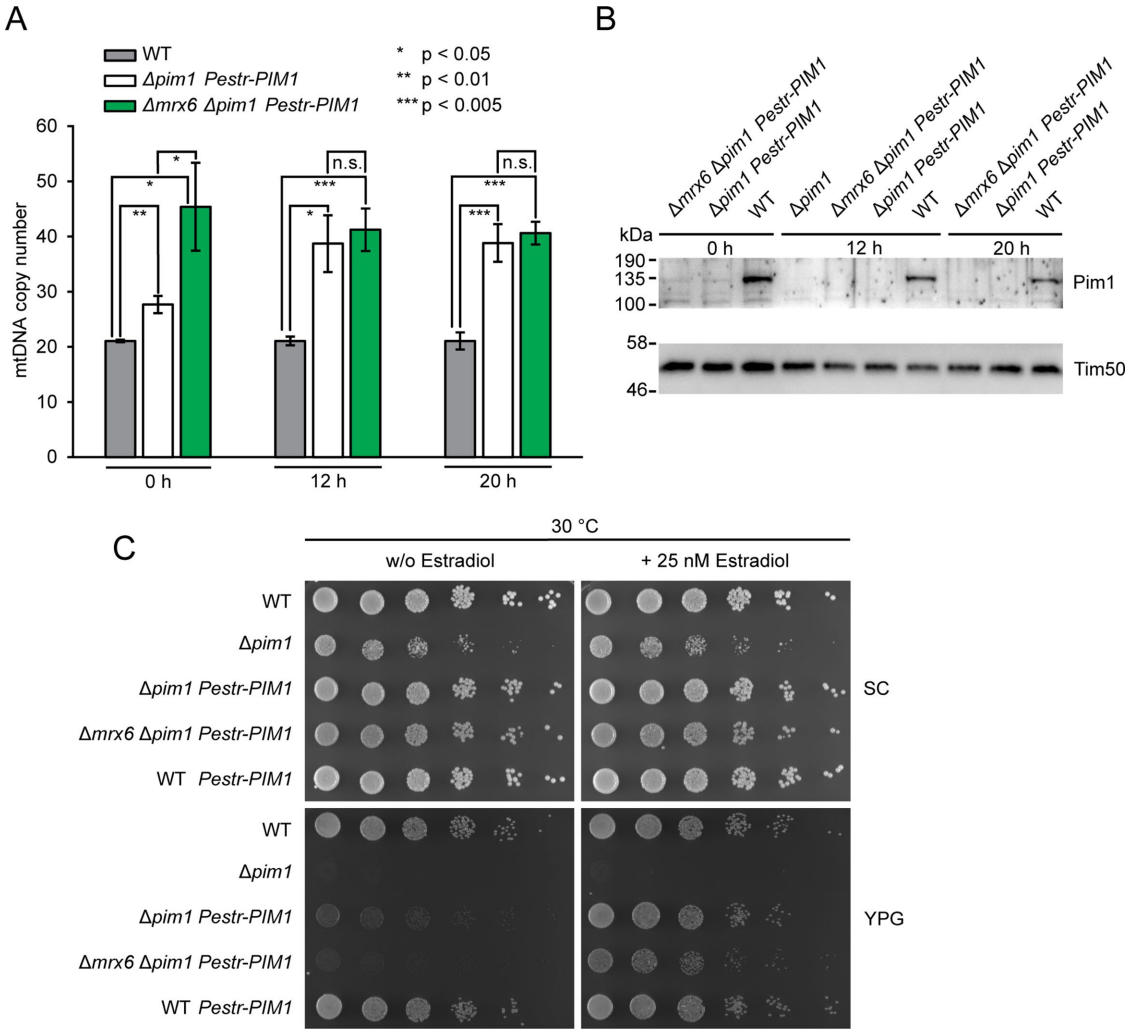

FIGURE 10: Acute depletion of Pim1 results in increased mtDNA copy number similar to levels of Δ*mrx6* cells, but does not further exceed these levels in the double mutant. (A) qPCR analyses of mtDNA copy number in cells that harbor an estradiol-inducible Pim1 expression construct and lack either only *PIM1* (Δ*pim1 Pestr*-PIM1) or both *PIM1* and *MRX6* (Δ*mrx6* Δ*pim1 Pestr*-PIM1). Estradiol (25 nM) was supplied for Pim1 expression and omitting estradiol from the medium induced acute depletion of Pim1. Cells were continuously maintained at log phase in SC medium and harvested at OD_{600} = 1 at the respective time points for DNA extraction (n = 3 with three technical replicates each). (B) Western blot analyses of Pim1 levels in estradiol-regulatable strains and WT. The cells harvested for A were used for this experiment as well. (C) Drop dilution growth analysis of estradiol-inducible Pim1 strains in comparison to WT and Δ*pim1*. The 11,200 cells were serially diluted at a ratio of 1:5 and the dilutions were spotted on fermentable (SC-medium) and nonfermentable carbon sources (YPG-medium) supplemented with 25 nM estradiol or not, and cultivated for 2 d at 30°C.

the flow cytometer. The SSC-H parameter was used as an estimate of cell size, and the SSC-H values of the mutants were normalized to the value of WT. Cell size of some mutants was also analyzed by microscopy to verify cell size increase. The remaining cultures were used for gDNA isolation and subjected to qPCR for mtDNA analysis for Figure 1D.

Growth analysis

Yeast cells were grown in liquid media (YPD) in log phase for 24 h at 30°C and diluted to OD_{600} = 0.05 in total 100 µl YPD or diluted to OD_{600} = 0.1 in a total of 100 µl YPEG in a 96-well clear-bottomed microplate (Corning). The wells at the edges of the plate were filled with YPD to maintain humidity and the lid was secured using a tape that partially covered the plate to allow air exchange. Growth assays were conducted at 30°C using a Tecan Infinite 200 Pro plate reader for 48 h with a kinetic interval of 15 min.

Immunoprecipitation

Immunoprecipitations were performed as previously described (Friedman *et al.*, 2015). Briefly, 500 OD_{600} cells grown in log phase in YPD at 30°C were harvested by centrifugation and resuspended in 5 ml of lysis buffer (20 mM HEPES, pH 7.4, 150 mM KOAc, 2 mM $Mg(OAc)_2$, 1 mM EGTA [ethylene glycol-bis(β-aminoethyl ether)-*N*,*N*,*N*′,*N*′-tetraacetic acid], 0.6 M sorbitol), and protease inhibitor cocktail was added to 1x (EDTA-free; Roche). Cell suspension was flash-frozen dropwise in liquid N_2 and lysed using a ball mill (Retsch MM301). The cell powder was thawed at RT, and unbroken cells and large debris were pelleted using a GH-3.8 rotor at 1500 rpm for 5 min at 4°C. For solubilization, digitonin was added to the supernatant to a final concentration of 1%. Samples were incubated for 30 min at 4°C and cleared by centrifugation at 12,000 × *g* at 4°C. µMACS anti-Flag beads (Miltenyi Biotec; 50 µl) were added to the supernatant and incubated for 45 min at 4°C, followed by isolation

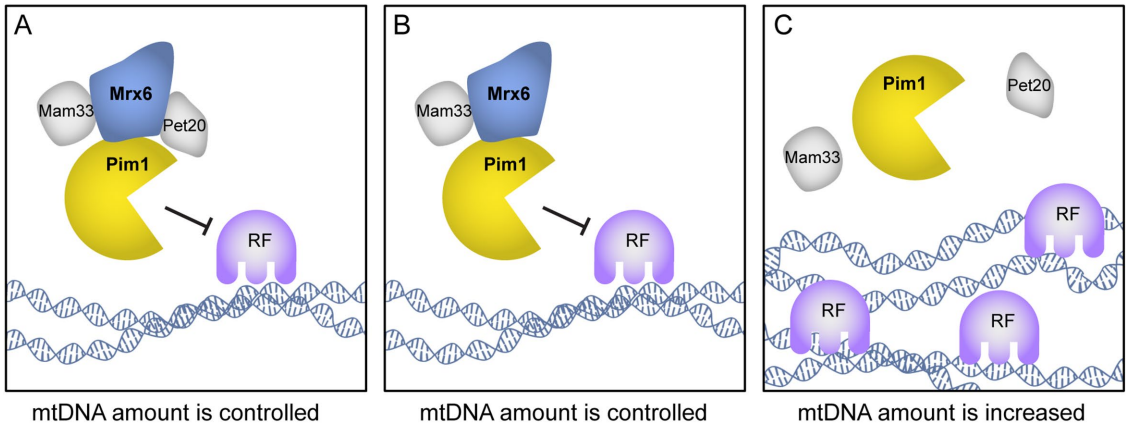

FIGURE 11: Model for the role of the Mrx6 complex in mtDNA replication. (A) The Mrx6 complex colocalizes preferentially with mtDNA, whereas single components are more often found in areas that lack mtDNA. (B) Mrx6 is essential for the formation of a Pim1-containing complex that controls mtDNA levels, whereas Pet20 is dispensable for sufficient mtDNA copy number control. (C) We propose that Mrx6 may facilitate substrate recognition of Pim1 and degradation of replication factors (RF) that stimulate mtDNA replication. Accordingly, absence of Mrx6 would lead to accumulation of such factors and result in increased amounts of mtDNA.

with µ columns and a µMACS separator (Miltenyi Biotec). Columns were washed three times with lysis buffer, 0.1% digitonin, and 1x protease inhibitor and two times with only lysis buffer. Samples were eluted using on-bead trypsin digest by incubating beads with 25 µl of elution buffer I (2M urea, 50 mM Tris-HCl, pH 7.5, 1 mM DTT, and 5 µg/ml trypsin [Trypsin Gold, Promega]) for 30 min at RT. Elution buffer II (50 µl; 2 M urea, 50 mM Tris-HCl, pH 7.5, 5 mM chloroacetamide) was added to the column two times to collect elutions. Elutions were kept at RT overnight to continue digestion. Mass spectrometric proteomic analysis was performed at the Genome Center Proteomics Core of the University of California, Davis.

Western blot analysis

For Figure 7A, the samples eluted from the µMACS beads by incubating beads with preheated (95°C) 1x SDS loading buffer instead of trypsin digestion. For Figure 2A and Supplemental Figure 8, proteins were extracted from 1 OD_{600} cells in urea-CHAPS buffer (20 mM Tris-HCl, pH 7.4, 7 M urea, 2 M thiourea, 4% CHAPS) by 3 min bead beating at 4°C. The protein concentration of each sample was measured by Pierce BCA protein assay kit (Thermo Scientific). Samples were boiled for 5 min in SDS loading dye and BME (β-mercaptoethanol) before SDS–PAGE analysis, transferred to nitrocellulose membrane, and immuno-blotted with the following primary antibodies at the indicated concentrations in 5% milk PBS-T (phosphate-buffered saline, 0.1% Tween 20)/TBS-T (Tris-buffered saline, 0.1% Tween 20) buffer: mouse anti-FLAG M2 (1:5000; Sigma–Aldrich); rabbit anti-Pim1 (1:1000; kindly provided by C. Suzuki, New Jersey Medical School, Rutgers, The State University of New Jersey); mouse anti-myc 9E10 (1:1000; Santa Cruz); mouse anti-PGK1 (1:5000; abcam); rabbit anti-Tom40 (1:30,000; kindly provided by T. Langer, Max-Planck-Institute for Biology of Ageing, Cologne, Germany); rabbit anti-Abf2 (1:1000; kindly provided by J. Nunnari, Department of Molecular and Cellular Biology, University of California, Davis, Davis, CA); rabbit anti-Tim50 (Mokranjac *et al.*, 2003) (1:1000; kindly provided by K. Hell, Biomedical Center Munich–Physiological Chemistry, Ludwig-Maximilians University, Planegg, Martinsried, Germany).

Structured illumination microscopy and analysis

For Figure 3A, slides were prepared as previously described (Kaplan and Ewers, 2015). Briefly, microscope coverslips (High Precision) were cleaned with a plasma cleaner (PDC-001, Harrick Plasma) and treated with concanavalin A (Sigma; 5 mg/ml) for 30 min, spin-coated for 15 s, and air-dried for 15 min in a vacuum desiccator. Before imaging, yeast cells were grown in liquid dropout synthetic media in log phase for 24 h at 30°C. A sample of 0.5 OD_{600} cells was spun down, washed, and resuspended in 100 µl PBS. A cell suspension (20 µl) was added on the concanavalin A–treated coverslips and incubated for 15 min. Unattached cells were washed with PBS. For fixation, cells were incubated twice for 5 min with 4% paraformaldehyde (Electron Microscopy Sciences) in PBS on coverslips. Fixation was followed by quenching two times with 50 mM NH_4Cl, 10 min each. Cells were washed with PBS and a drop of anti-fade medium (Vectashield) was added before mounting coverslips to slides. Slides were imaged using DeltaVision OMX SR (GE) using SIM mode and a 60x/1.42 NA oil objective. The Imaris software was used to detect/count LacI-GFP foci and to segment the mitochondrial network in three dimensions. Quantification of mitochondrial network length, mitochondrial endpoints, and distribution of mtDNA was performed as described previously (Osman *et al.*, 2015). Three- or four-way junctions of the segmented mitochondrial network were scored as branchpoints.

For Figure 4A, yeast cells were grown in liquid dropout synthetic media in log phase for 24 h at 30°C and fixed with 4% paraformaldehyde (Electron Microscopy Sciences) in growth media for 30 min at RT. Cells were prepared as described previously (Silver, 2009). Briefly, cells were pelleted and washed two times with P solution (0.1 M $KHPO_4$, 1.2 M sorbitol) and resuspended in 1 ml of P solution. After 15 µl of 10 mg/ml zymolyase (T-20) and 5 µl BME were added to the solution it was incubated at RT for 30 min. Cells were gently washed once with P solution and resuspended in 0.5 ml of P solution. Microscope coverslips (High Precision) were plasma-cleaned and coated with 0.1% poly-L-lysine for 20 min. Coverslips were washed two times with ddH_2O and air-dried completely. Cell suspension (30 µl) was added and incubated 20 min. Excess media were aspirated and coverslips were plunged into ice-cold methanol for 6 min, followed by submergence into ice-cold acetone for 30 s. Coverslips were air-dried briefly and incubated with 3% bovine serum albumin (BSA) (Sigma) in PBS for 1 h at RT. Cells were stained with DAPI (Invitrogen; 5 µg/ml) for 5 min and washed two times with PBS. Coverslips were mounted on

slides after addition of a drop of anti-fade medium (Vectashield). Slides were imaged using DeltaVision OMX SR (GE) using SIM mode and a 60x/1.42 NA oil objective. The Imaris software was used to calculate the number of DAPI-stained nucleoids and the volume of each nucleoid in three dimensions.

Immunofluorescence and analysis

Cells were prepared for immunofluorescence as was done before for the cells shown in Figure 4A, except that after acetone treatment cells were incubated with blocking buffer, 3% goat serum (Jackson ImmunoResearch) in PBS for 1 h at RT, followed by incubation with mouse anti-DNA antibody (1:1000; abcam) in blocking buffer overnight at 4°C. The next day, cells were washed three times with blocking buffer and incubated with anti-mouse secondary antibody conjugated with Alexa Fluor 405 (1:500) or Alexa Fluor 647 (1:1000) for an hour and a half at RT in the dark. Subsequently, cells were washed three times with blocking buffer and two times with PBS, and if necessary stained with DAPI (5 µg/ml) for 5 min and washed two times with PBS. Coverslips were mounted on slides after addition of a drop of anti-fade medium (Vectashield). Slides were imaged using DeltaVision OMX SR (GE) using conventional mode and a 60x/1.42 NA oil objective. Deconvolution of images and maximum projection of Z stacks were done using DeltaVision SoftWorRx. Quantification of nucleoid length was performed as follows. First a curved line was manually drawn through the mitochondrial network of each cell and the line's one-dimensional intensity profile was extracted. Then nucleoids were automatically picked out from the intensity profile by adaptive thresholding. Local threshold values were individually calculated for data points using Li's minimum cross-entropy method applied within a 4.8-µm-long sliding window (Li and Lee, 1993). The sliding-window approach allowed us to compensate for nonuniform fluorescent background in the images and to robustly identify peaks in the intensity profile in an unbiased way (Supplemental Figure 3A). We carried out our experiments to determine the length of nucleoids using both conventional and super-resolution (structured illumination) microscopy (Figure 4) and found that the increase in nucleoid length in Δ*mrx6* cells was robustly detected by both methods.

Live microscopy and analysis

Microscope coverslips (High Precision) were plasma-cleaned and treated with concanavalin A (0.5 mg/ml) for 15 min, spin-coated for 15 s, and air-dried for 15 min in a vacuum desiccator. Before imaging, yeast cells were grown in liquid dropout synthetic media in log phase for 24 h. DAPI was added to media (final concentration 1 µg/ml) for 15 min if needed. Samples of 0.5 OD_{600} cells were spun down, washed, and resuspended in 20 µl dropout synthetic media lacking sugar. Cell suspension was added on the concanavalin A–treated cover slips and incubated for 5 min. Unattached cells were washed with dropout synthetic media. Slides were imaged using DeltaVision OMX SR (GE) using conventional mode and a 60x/1.42 NA oil objective. Deconvolution of images and maximum projection of Z stacks were done using DeltaVision softWoRx. Intensity profiles were obtained with ImageJ by measuring pixel intensities along mitochondrial tubules of Z-projected images using the line draw tool (settings: linewidth = 3). Intensity profiles along identical lines from different channels were used to calculate the PCCs (Supplemental Figure 5C). The MCCs were calculated after thresholding intensity profiles using Yen's method (Yen *et al.*, 1995). To assess the significance of colocalizations, MCCs and PCCs were determined for intensity profiles of two channels, one of which was randomized by scrambling blocks of five values (400 nm) in the line profiles. Scrambling blocks of values rather than single values has been shown to give a more accurate probability distribution, because it retains autocorrelation between neighboring pixels (Costes *et al.*, 2004). Statistical significance of PCC and MCC values between measured and randomized intensity profiles was determined by applying the independent *t* test.

To test whether fractions of Mrx6 or Pet20 that colocalize with Pim1 preferentially colocalize with DAPI, intensity profiles for Mrx6-Neon or Pet20-Neon and Pim1-Ruby were first thresholded with Yen's method and then multiplied by one another. Values greater than 0 in the resulting profile were scored as colocalizing fractions, whereas values equal to 0 were scored as noncolocalizing fractions. MCC values between colocalizing or noncolocalizing fractions of Mrx6-Neon-Pim1-Ruby or Pet20-Neon-Pim1-Ruby and DAPI were determined as described in the preceding paragraph. To assess significance of this analysis, the same analysis was performed with a randomized DAPI profile. A *t* test was used to infer statistical significance between MCC values determined for the real data and the randomized data.

Acute depletion of Pim1

For expression of proteins under the control of an estradiol-regulatable expression system, we assembled pCO450 in multistep NEBuilder (New England Biolabs) cloning procedures. The previously reported plasmid encoded components of an established yeast estradiol expression system, "P*ACT1*(-1-520)-LexA-ER-haB42-T*CYC1*" (FPR718) and "insul-(*lexA*-box)2-Pmin*CYC1*-CitrineA206K-T*CYC1*" (FPR792; Ottoz *et al.*, 2014) were combined on one plasmid followed by an *Sph*I/*Nhe*I cloning site for integration of the target gene in combination with a KanMX6 selection marker. The construct was flanked with two homology regions that enable stable genomic integration into the yeast HO locus to omit irregular expressions within the culture owing to alterations in plasmid quantity in different cells. From this plasmid (pCO450), estradiol-regulatable Pim1-strains were generated by construction of pCO460. The open reading frame of *PIM1* was amplified from genomic DNA using the forward primer 5′-CTATACTAGTGGATCCGCATGCTAAGAACAAGAACCACAAAGA-3′ and the reverse primer 5′-CATAACTAATTACATGAGCTAGCGTTAGTCCTTTTCCTTTTTAGCATCCAA-3′ and introduced into the *Sph*I-linearized pCO450 backbone by the NEBuilder reaction. The resulting plasmid was linearized by *Not*I digestion and genomically integrated into the HO locus of WT cells (yCO363) by transformation and subsequent G418 selection (yCO575). The endogenous *PIM1* locus was deleted afterward via homologous recombination and a hygromycin marker as described previously (Janke *et al.*, 2004), resulting in yCO593. Strains were maintained continuously on medium containing β-estradiol (Alfa Aesar). By maintaining Pim1 expression, we could circumvent pleiotropic effects that manifest once the endogenous copy of *PIM1* is deleted. The double mutant yCO600 was generated by additionally deleting *MRX6* with a nourseothricin selection marker.

For experiments presented in Figure 10, cells were grown in liquid culture at log phase in synthetic complete medium containing 2% glucose supplemented with 25 nM β-estradiol. To acutely deplete Pim1 expression, cells were washed and estradiol was omitted from the medium. Cultures were permanently maintained in log phase and harvested at OD_{600} = 1 at each time point. For DNA and protein extraction, 2.5 OD_{600} cells were harvested, washed with Milli-Q water, and frozen immediately. Total DNA was extracted as previously reported by bead breaking in the presence of phenol/chloroform/isoamyl alcohol (Hoffman, 1997). The mtDNA copy

number was determined by quantitative PCR using iQ-Syber Green Supermix (Bio-RAD) as described in *Cell growth and quantitative PCR*.

ACKNOWLEDGMENTS

We thank Jodi Nunnari, David Morgan, Wallace Marshall, Patrick O'Farrell, and members of the Walter lab for their technical advice and insightful discussions. We thank Carolyn Suzuki for providing the anti-Pim1 antibody, Jodi Nunnari for the anti-Abf2 antibody, Thomas Langer for the anti-Tom40 antibody, Kai Hell for the anti-Tim50 antibody, Fabian Rudolf for plasmids FRP718 and FRP792, Voytek Okreglak, Hansong Ma, Jeiwei Xu, Jason Wojcechowskyj, Ingacio Zuleta, Ricardo Almeida, Amy Chang, Shoshana Brown, Samantha Lewis, and Justin M. Yamada for reagents, technical advice, and their helpful discussions, and Anne Pipathsouk and Roberto Diaz for their technical help during their rotation and internship, respectively. We thank Tanja Kautzleben for her technical assistance. We also thank the Nikon Imaging Center at the University of California, San Francisco, and Proteomics Core Facility at the University of California, Davis, for their invaluable contributions. This work was supported by a UCSF Zaffaroni Fellowship (to A.G.) and Howard Hughes Medical Institute (HHMI) International Student Research Fellowships (to A.G. and A.M.). V.B. is a Damon Runyon Fellow supported by the Damon Runyon Cancer Research Foundation (DRG-2284-17). C.O. was funded by the Simons Foundation (#326844). C.O. and S.S. are supported by a grant from the European Research Council (ERCStG-714739 IlluMitoDNA). P.W. is an HHMI Investigator.

REFERENCES

Bayot A, Gareil M, Rogowska-Wrzesinska A, Roepstorff P, Friguet B, Bulteau AL (2010). Identification of novel oxidized protein substrates and physiological partners of the mitochondrial ATP-dependent Lon-like protease Pim1. J Biol Chem 285, 11445–11457.

Brown TA, Tkachuk AN, Shtengel G, Kopek BG, Bogenhagen DF, Hess HF, Clayton DA (2011). Superresolution fluorescence imaging of mitochondrial nucleoids reveals their spatial range, limits, and membrane interaction. Mol Cell Biol 31, 4994–5010.

Chen XJ, Butow RA (2005). The organization and inheritance of the mitochondrial genome. Nat Rev Genet 6, 815–825.

Clay Montier LL, Deng JJ, Bai Y (2009). Number matters: control of mammalian mitochondrial DNA copy number. J Genet Genomics 36, 125–131.

Connelly CF, Akey JM (2012). On the prospects of whole-genome association mapping in *Saccharomyces cerevisiae*. Genetics 191, 1345–1353.

Conrad MN, Newlon CS (1982). The regulation of mitochondrial DNA levels in *Saccharomyces cerevisiae*. Curr Genet 6, 147–152.

Costes SV, Daelemans D, Cho EH, Dobbin Z, Pavlakis G, Lockett S (2004). Automatic and quantitative measurement of protein–protein colocalization in live cells. Biophys J 86, 3993–4003.

Ekstrand MI, Falkenberg M, Rantanen A, Park CB, Gaspari M, Hultenby K, Rustin P, Gustafsson CM, Larsson NG (2004). Mitochondrial transcription factor A regulates mtDNA copy number in mammals. Hum Mol Genet 13, 935–944.

Friedman JR, Mourier A, Yamada J, McCaffery JM, Nunnari J (2015). MICOS coordinates with respiratory complexes and lipids to establish mitochondrial inner membrane architecture. Elife 4, e07739.

Fukuoh A, Cannino G, Gerards M, Buckley S, Kazancioglu S, Scialo F, Lihavainen E, Ribeiro A, Dufour E, Jacobs HT (2014). Screen for mitochondrial DNA copy number maintenance genes reveals essential role for ATP synthase. Mol Syst Biol 10, 734.

Giaever G, Chu AM, Ni L, Connelly C, Riles L, Véronneau S, Dow S, Lucau-Danila A, Anderson K, André B, *et al*. (2002). Functional profiling of the *Saccharomyces cerevisiae* genome. Nature 418, 387–391.

Hoffman CS (1997). Preparation of yeast DNA. Curr Protoc Mol Biol 39, 13.11.11–13.11.14.

Ikeda M, Ide T, Fujino T, Arai S, Saku K, Kakino T, Tyynismaa H, Yamasaki T, Yamada K, Kang D, *et al*. (2015). Overexpression of TFAM or twinkle increases mtDNA copy number and facilitates cardioprotection associated with limited mitochondrial oxidative stress. PLoS One 10, e0119687.

Jajoo R, Jung Y, Huh D, Viana MP, Rafelski SM, Springer M, Paulsson J (2016). Accurate concentration control of mitochondria and nucleoids. Science 351, 169–172.

Janke C, Magiera MM, Rathfelder N, Taxis C, Reber S, Maekawa H, Moreno-Borchart A, Doenges G, Schwob E, Schiebel E, Knop M (2004). A versatile toolbox for PCR-based tagging of yeast genes: new fluorescent proteins, more markers and promoter substitution cassettes. Yeast 21, 947–962.

Jonas K, Liu J, Chien P, Laub MT (2013). Proteotoxic stress induces a cell-cycle arrest by stimulating Lon to degrade the replication initiator DnaA. Cell 154, 623–636.

Kanki T, Ohgaki K, Gaspari M, Gustafsson CM, Fukuoh A, Sasaki N, Hamasaki N, Kang D (2004). Architectural role of mitochondrial transcription factor A in maintenance of human mitochondrial DNA. Mol Cell Biol 24, 9823–9834.

Kaplan C, Ewers H (2015). Optimized sample preparation for single-molecule localization-based superresolution microscopy in yeast. Nat Protoc 10, 1007–1021.

Kaufman BA, Kolesar JE, Perlman PS, Butow RA (2003). A function for the mitochondrial chaperonin Hsp60 in the structure and transmission of mitochondrial DNA nucleoids in *Saccharomyces cerevisiae*. J Cell Biol 163, 457–461.

Kehrein K, Schilling R, Moller-Hergt BV, Wurm CA, Jakobs S, Lamkemeyer T, Langer T, Ott M (2015). Organization of mitochondrial gene expression in two distinct ribosome-containing assemblies. Cell Rep 10, 843–853.

Kleinman MJ (1996). Yeast colony hybridization. Methods Mol Biol 53, 189–192.

Kornblum C, Nicholls TJ, Haack TB, Schöler S, Peeva V, Danhauser K, Hallmann K, Zsurka G, Rorbach J, Iuso A, *et al*. (2013). Loss-of-function mutations in MGME1 impair mtDNA replication and cause multisystemic mitochondrial disease. Nat Genet 45, 214.

Kukat C, Wurm CA, Spåhr H, Falkenberg M, Larsson N-G, Jakobs S (2011). Super-resolution microscopy reveals that mammalian mitochondrial nucleoids have a uniform size and frequently contain a single copy of mtDNA. Proc Natl Acad Sci USA 108, 13534–13539.

Kunova N, Ondrovicova G, Bauer JA, Bellova J, Ambro L, Martinakova L, Kotrasova V, Kutejova E, Pevala V (2017). The role of Lon-mediated proteolysis in the dynamics of mitochondrial nucleic acid–protein complexes. Sci Rep 7, 631.

Langklotz S, Narberhaus F (2011). The *Escherichia coli* replication inhibitor CspD is subject to growth-regulated degradation by the Lon protease. Mol Microbiol 80, 1313–1325.

Lewis SC, Uchiyama LF, Nunnari J (2016). ER-mitochondria contacts couple mtDNA synthesis with mitochondrial division in human cells. Science 353, aaf5549.

Li CH, Lee CK (1993). Minimum cross entropy thresholding. Pattern Recogn 26, 617–625.

Lipinski KA, Kaniak-Golik A, Golik P (2010). Maintenance and expression of the *S.cerevisiae* mitochondrial genome—from genetics to evolution and systems biology. Biochim Biophys Acta 1797, 1086–1098.

Liu C-S, Cheng W-L, Lee C-F, Ma Y-S, Lin C-Y, Huang C-C, Wei Y-H (2006). Alteration in the copy number of mitochondrial DNA in leukocytes of patients with mitochondrial encephalomyopathies. Acta Neurol Scand 113, 334–341.

Lu B, Lee J, Nie X, Li M, Morozov YI, Venkatesh S, Bogenhagen DF, Temiakov D, Suzuki CK (2013). Phosphorylation of human TFAM in mitochondria impairs DNA binding and promotes degradation by the AAA+ Lon protease. Mol Cell 49, 121–132.

Lu B, Yadav S, Shah PG, Liu T, Tian B, Pukszta S, Villaluna N, Kutejova E, Newlon CS, Santos JH, Suzuki CK (2007). Roles for the human ATP-dependent Lon protease in mitochondrial DNA maintenance. J Biol Chem 282, 17363–17374.

MacAlpine DM, Perlman PS, Butow RA (2000). The numbers of individual mitochondrial DNA molecules and mitochondrial DNA nucleoids in yeast are co-regulated by the general amino acid control pathway. EMBO J 19, 767–775.

Major T, von Janowsky B, Ruppert T, Mogk A, Voos W (2006). Proteomic analysis of mitochondrial protein turnover: identification of novel substrate proteins of the matrix protease pim1. Mol Cell Biol 26, 762–776.

Matsushima Y, Goto Y, Kaguni LS (2010). Mitochondrial Lon protease regulates mitochondrial DNA copy number and transcription by selective degradation of mitochondrial transcription factor A (TFAM). Proc Natl Acad Sci USA 107, 18410–18415.

Meeusen S, Nunnari J (2003). Evidence for a two membrane-spanning autonomous mitochondrial DNA replisome. J Cell Biol 163, 503–510.
Mengel-From J, Thinggaard M, Dalgård C, Kyvik KO, Christensen K, Christiansen L (2014). Mitochondrial DNA copy number in peripheral blood cells declines with age and is associated with general health among elderly. Hum Genet 133, 1149–1159.
Miller FJ, Rosenfeldt FL, Zhang C, Linnane AW, Nagley P (2003). Precise determination of mitochondrial DNA copy number in human skeletal and cardiac muscle by a PCR-based assay: lack of change of copy number with age. Nucleic Acids Res 31, e61.
Mokranjac D, Paschen SA, Kozany C, Prokisch H, Hoppins SC, Nargang FE, Neupert W, Hell K (2003). Tim50, a novel component of the TIM23 preprotein translocase of mitochondria. EMBO J 22, 816–825.
Osman C, Noriega TR, Okreglak V, Fung JC, Walter P (2015). Integrity of the yeast mitochondrial genome, but not its distribution and inheritance, relies on mitochondrial fission and fusion. Proc Natl Acad Sci USA 112, E947–E956.
Ottoz DS, Rudolf F, Stelling J (2014). Inducible, tightly regulated and growth condition-independent transcription factor in Saccharomyces cerevisiae. Nucleic Acids Res 42, e130.
Picchioni D, Antolin-Fontes A, Camacho N, Schmitz C, Pons-Pons A, Rodríguez-Escribà M, Machallekidou A, Güler MN, Siatra P, Carretero-Junquera M, *et al*. (2019). Mitochondrial protein synthesis and mtDNA levels coordinated through an aminoacyl-tRNA synthetase subunit. Cell Rep 27, 40–47.e45.
Polevoda B, Panciera Y, Brown SP, Wei J, Sherman F (2006). Phenotypes of yeast mutants lacking the mitochondrial protein Pet20p. Yeast 23, 127–139.
Pyle A, Anugrha H, Kurzawa-Akanbi M, Yarnall A, Burn D, Hudson G (2016). Reduced mitochondrial DNA copy number is a biomarker of Parkinson's disease. Neurobiol Aging 38, 216 e217–216 e210.
Rafelski SM, Viana MP, Zhang Y, Chan YH, Thorn KS, Yam P, Fung JC, Li H, Costa Lda F, Marshall WF (2012). Mitochondrial network size scaling in budding yeast. Science 338, 822–824.
Roloff GA, Henry MF (2015). Mam33 promotes cytochrome c oxidase subunit I translation in *Saccharomyces cerevisiae* mitochondria. Mol Biol Cell 26, 2885–2894.
Silver P (2009). Indirect immunofluorescence labeling in the yeast Saccharomyces cerevisiae. Cold Spring Harb Protoc *2009*, pdb prot5317.
Taylor SD, Zhang H, Eaton JS, Rodeheffer MS, Lebedeva MA, O'Rourke T, Siede W, Shadel GS (2005). The conserved Mec1/Rad53 nuclear checkpoint pathway regulates mitochondrial DNA copy number in *Saccharomyces cerevisiae*. Mol Biol Cell 16, 3010–3018.
Traven A, Janicke A, Harrison P, Swaminathan A, Seemann T, Beilharz TH (2012). Transcriptional profiling of a yeast colony provides new insight into the heterogeneity of multicellular fungal communities. PLoS One 7, e46243.
Ulery TL, Jang SH, Jaehning JA (1994). Glucose repression of yeast mitochondrial transcription: kinetics of derepression and role of nuclear genes. Mol Cell Biol 14, 1160–1170.
Venkatesh S, Lee J, Singh K, Lee I, Suzuki CK (2012). Multitasking in the mitochondrion by the ATP-dependent Lon protease. Biochim Biophys Acta 1823, 56–66.
Wei J, Sherman F (2004). Sue1p is required for degradation of labile forms of altered cytochromes C in yeast mitochondria. J Biol Chem 279, 30449–30458.
Williams RS (1986). Mitochondrial gene expression in mammalian striated muscle. Evidence that variation in gene dosage is the major regulatory event. J Biol Chem 261, 12390–12394.
Yen JC, Chang FJ, Chang S (1995). A new criterion for automatic multilevel thresholding. IEEE Trans Image Process 4, 370–378.
Ylikallio E, Tyynismaa H, Tsutsui H, Ide T, Suomalainen A (2010). High mitochondrial DNA copy number has detrimental effects in mice. Hum Mol Genet 19, 2695–2705.
Yu M (2011). Generation, function and diagnostic value of mitochondrial DNA copy number alterations in human cancers. Life Sci 89, 65–71.
Zelenaya-Troitskaya O, Newman SM, Okamoto K, Perlman PS, Butow RA (1998). Functions of the high mobility group protein, Abf2p, in mitochondrial DNA segregation, recombination and copy number in *Saccharomyces cerevisiae*. Genetics 148, 1763–1776.
Zhang H, Singh KK (2014). Global genetic determinants of mitochondrial DNA copy number. PLoS One 9, e105242.